Hydrogen double compression-expansion engine (H2DCEE): A sustainable internal combustion engine with 60%+ brake thermal efficiency potential at

Energy Conversion and Management 264 (2022) 115698

Contents lists available at ScienceDirect

Energy Conversion and Management

journal homepage: www.elsevier.com/locate/enconman

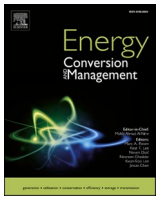

Hydrogen double compression-expansion engine (H2DCEE): A sustainable internal combustion engine with 60%+ brake thermal efficiency potential at 45 bar BMEP

Rafig Babayev [a,*], Hong G. Im [b], Arne Andersson [c], Bengt Johansson [a]

[a] Combustion Engine Research Center (CERC), Chalmers University of Technology, Sweden
[b] Clean Combustion Research Center (CCRC), King Abdullah University of Science and Technology (KAUST), Saudi Arabia
[c] Powertrain Strategic Development (PSD), Volvo Group Trucks Technology (Volvo GTT), Sweden

ARTICLE INFO

Keywords:
Hydrogen combustion
Direct injection
Compression ignition
Hydrogen engine
High efficiency
CFD

ABSTRACT

Hydrogen (H_2) internal combustion engines may represent cost-effective and quick solution to the issue of the road transport decarbonization. A major factor limiting their competitiveness relative to fuel cells (FC) is the lower efficiency. The present work aims to demonstrate the feasibility of a H_2 engine with FC-like 60%+ brake thermal efficiency (BTE) levels using a double compression-expansion engine (DCEE) concept combined with a high pressure direct injection (HPDI) nonpremixed H_2 combustion. Experimentally validated 3D CFD simulations are combined with 1D GT-Power simulations to make the predictions. Several modifications to the system design and operating conditions are systematically implemented and their effects are investigated. Addition of a catalytic burner in the combustor exhaust, insulation of the expander, dehumidification of the EGR, and removal of the intercooling yielded 1.5, 1.3, 0.8, and 0.5%-point BTE improvements, respectively. Raising the peak pressure to 300 bar via a larger compressor further improved the BTE by 1.8%-points but should be accompanied with a higher injector-cylinder differential pressure. The λ of ~1.4 gave the optimum tradeoff between the mechanical and combustion efficiencies. A peak BTE of 60.3% is reported with H2DCEE, which is ~5%-points higher than the best diesel-fueled DCEE alternative.

1. Introduction

Hydrogen (H_2) fuel is once again viewed as a promising energy carrier that could enable a rapid decarbonization of the transport sector. As of 2022, an unprecedented momentum in the field of H_2 technologies is observed on a global scale, driven by strong economic and political forces. Approximately USD 500 billion in investments is expected by 2030, based on ~ 360 large-scale projects globally announced across the value chain [1]. About 30%, or USD 150 billion is associated with mature projects, which have already passed the final investment decision or are under construction, commissioning, or operation.

For the transport applications, to convert the chemical energy bound in the H_2 fuel into useful mechanical work, either a fuel cell (FC) system or an internal combustion engine (ICE) system can be used. FC vehicles currently have the advantage of a higher thermal efficiency and no tailpipe emissions, while facing issues with FC stack durability and lifespan [2], high cooling and "engine-braking" power requirements [3], and currently high cost of manufacturing [4] and ownership [5]. On the other hand, H_2 ICEs may produce significant NOx emissions, which require strict limitations on the combustion system design, and potentially the use of complex aftertreatment systems.

H_2 ICEs operating on the port fuel injected (PFI) spark-ignition (SI) principle, being at a higher technology readiness level, are relatively well studied [6–13]. However, they are limited in power density and maximum load due to the displacement of air by the H_2 gas in the engine intake, and in efficiency owing to H_2 fuel's proclivity to preignition and knocking [14–16]. Direct-injection (DI) H_2 fueling systems [16–19] can improve the power density but cannot address the efficiency issue. The high knocking tendency is caused by H_2's low ignition energy (e.g., 0.017 mJ for H_2 versus 0.29 mJ for CH_4 [7]), wide flammability range (e.g., $0.10 < \varphi < 7.14$ for H_2 versus $0.50 < \varphi < 1.67$ for CH_4 [20,21]), and high flame speeds (e.g., ~230 cm/s for H_2 versus 42 cm/s for CH_4 at ambient conditions and $\varphi = 0.6$–0.7). This often necessitates the use of very lean fuel–air mixtures, which limits the engine efficiency and load even with DI fueling systems in the SI mode.

* Corresponding author at: Division of Combustion and Propulsion Systems, Hörsalsvägen 7B, SE-412 96, Göteborg, Sweden.
E-mail address: rafig.babayev@volvo.com (R. Babayev).

https://doi.org/10.1016/j.enconman.2022.115698
Received 6 February 2022; Received in revised form 17 April 2022; Accepted 29 April 2022
Available online 19 May 2022

Nomenclature

Definitions/Abbreviations

%-point	percentage point
AMR	adaptive mesh refinement
aTDC	after top dead center
BMEP	brake mean effective pressure
BTE	brake thermal efficiency
CA°	crank angle degrees
CAC	charge air cooler
CFD	computational fluid dynamics
CI	compression ignition
CR	compression ratio
DCEE	double compression-expansion engine
EGR	exhaust gas recirculation
EVC	exhaust valve closing
FC	fuel cell
GE	gas exchange
GIW	gross indicated work
HP	high-pressure
HPDI	high pressure direct injection
HTM	heat transfer multiplier
ICE	internal combustion engine
IVC	inlet valve closing
LP	low-pressure
NIW	neat indicated work
PCP	peak cylinder pressure (with combustion)
PMP	peak motoring pressure (without combustion)
SCR	selective catalytic reduction
SOI	start of injection
TDC	top dead center
γ	specific heat ratio
η_{comb}	combustion efficiency
λ	air–fuel equivalence ratio

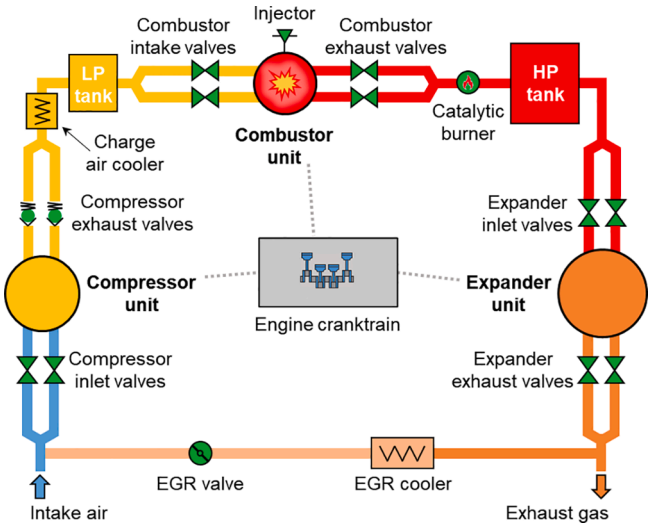

Fig. 1. 1D GT-Power model layout for the double compression-expansion engine (DCEE).

In our previous studies, we have shown that a compression-ignition (CI) nonpremixed combustion of H_2 can be used instead of the SI approach in H_2 ICEs to eliminate knocking and enable higher efficiencies and power densities [22–24]. Other authors have also demonstrated successful CI H_2 engine operation experimentally [25–29] and numerically [30–32]. Building upon this knowledge, the present work will demonstrate that H_2 ICE based powertrains may also match and even surpass FC based powertrains in efficiency. This will be achieved with the help of a double compression-expansion engine (DCEE) concept that would use, as its base platform, a slightly modified Volvo D13 heavy-duty engine fueled with H_2. This combination (H_2 + DCEE) has already been introduced in [33], and its most important benefits over the conventional diesel combustion were highlighted to be the following: (1) net molar expansion due to the H_2 injection at TDC, which contributes additional 2–4% of fuel energy to useful work, (2) the lack of soot-NOx tradeoff allows for extreme NOx minimization strategies, as well as reduced jet momentum to minimize wall heat transfer losses, (3) possibility of using selective catalytic reduction (SCR) systems with H_2 as a reducing agent instead of ammonia to greatly simplify the system. The present work will focus on improving the H2DCEE system efficiency at a high-load operating point (~45 bar BMEP), achieving a brake thermal efficiency (BTE) comparable to that with FC powertrains operating at low-to-medium loads, up to ~60% BTE. In this study, several modifications are systematically implemented, and the effects of each are carefully studied.

The operating principle of the DCEE system that would enable FC levels of thermal efficiency is described in the following. The concept consists of three dedicated cylinders: compressor, combustor, and expander units. The compressor charges the low-pressure (LP) accumulator tank, which then feeds the combustor unit. The combustor is a regular heavy-duty Volvo D13 engine with only few modifications which are described in Section 2. The exhaust gases from the combustor unit are passed into the high-pressure (HP) accumulator tank, which then feeds the expander unit. The operating principle is overall similar to a regular turbocharged diesel engine. The difference is that the compressor and expander are piston machines, which has a few important advantages. These include the possibility of large pressure ratios over the compressor, hence high boosting levels for the combustor unit at lower compression ratios (CR), which allows for more flexibility in optimizing the system for higher efficiency and lower emissions. Piston compressors also allow for high levels of humidity, which enables the use of a long-route exhaust gas recirculation (EGR) system with H_2 combustion for further improved efficiency. For the expansion, the two-stage process (first in the combustor, then in the expander) also allows for better optimization, easier and more effective heat insulation, and overexpansion for improved thermodynamic efficiency. The highly effective insulation of the second-stage expansion is possible owing to the expander unit's special design, while the combustor unit can also be minimized in size to limit heat losses. The sustained high temperatures in the HP tank also allows for more effective and cheaper aftertreatment systems, while the expander unit can even be used for ammonia injections. Multiple experimental and computational studies [33–38] have demonstrated that the DCEE fueled with diesel can achieve about 55% BTE.

The present article aims to computationally implement several system modifications primarily targeted at maximizing engine efficiency within certain operational and emission limits. This has not been attempted before, as the previous H2DCEE study [33] only focused on preliminary screening of the system performance. The current paper starts by providing a detailed description of the H2DCEE system setup and operating conditions (Section 2) and a description of the 1D CFD system model and 3D CFD combustion cylinder model (Sections 3 and 4, respectively). Then, the sector modeling approach is validated against the full-geometry full-cycle simulations (Section 5). Subsequently, the details of the different parametric cases of the study are given in Section 6. The results of the parametric studies are presented and discussed in

Section 7, starting from the effects of each modification on the system at lower pressures (Sections 7.1-7.6). Subsequently, the effects of raising the peak system pressures on the combustion system are studied in detail in Section 7.7, while the effects on the entire DCEE system are studied in Sections 7.8. Finally, the H2DCEE is compared to its diesel equivalent in Appendix B, and all the notable conclusions of this work are summarized in Section 8.

2. DCEE system setup and operating conditions

As shown in the system layout diagram in Fig. 1, the DCEE consists of three dedicated cylinders: compressor, combustor, and expander units, all connected to a single crank mechanism, and their phasing is offset by 180°. Figure C. 1 in the Appendix also provides the layout as it appears in the GT-Power software GUI. The compressor and expander are two-stroke machines, while the combustor is assumed to be identical to the regular four-stroke Volvo D13 heavy-duty engine. The compression ratio (CR) of the combustor unit in the DCEE concept is 11.7:1, as opposed to 17:1 in the standard D13 engine. This is because more work production is allocated to the low-pressure part of the cycle, i.e., expander. For combustion cylinder specifications, see Table A1 in the Appendix. Ignition is achieved via higher intake temperatures (at least 420 K at BDC) with less or no intercooling, and neat hydrogen pilot injections, which help achieve ignition at lower temperatures (for details, see [23]).

A high-pressure direct-injection (HPDI) gas injector is computationally incorporated into the system. The injector nozzle was modified from the original natural gas version to compensate for hydrogen's lower density, as well as to optimize the combustion system for jet mixing dominated nonpremixed H_2 combustion. The number of nozzle orifices was increased up to 12, the umbrella angle was set at 154°, and the orifice diameter was set at 1 mm. The H_2 fuel injection rate profile was assumed to be the same in all cases for better comparison, and the profile was taken from the Generation 4 DICI H_2 combustion case in Babayev et al. [24]. The injection rate corresponds to approximately 70 bar differential pressure between the injector and the cylinder. All these modifications helped improve the nonpremixed H_2 combustion process, achieving higher heat release rates and lower wall heat transfer. For details on the optimization approach, refer to [24]. The injection rate is shown in Fig. 7, where the pilot SOI is at −10 CA° aTDC at lower cylinder pressures and −2 CA° aTDC at higher pressures. The main injection SOI is always at TDC, and the injection duration is 9.2 CA°.

The geometrical CR of the compressor and expander units is 158:1. The high-CR pistons can be coupled with a cam-less variable valve actuation system [39] to ensure precise and safe operation. Note that, the intake valve closing (IVC) timing of the compressor and exhaust valve closing (EVC) timing of the expander are set late in the cycle, during the compression stroke. This limits the effective CR (pressure-based) of the units at approximately 15:1 and prevents excessively high peak pressures, while simultaneously minimizing the compression and unconstrained expansion losses by allowing for the high geometrical CR. The bore size of the compressor and expander units is adjusted for each generation of the DCEE system, and the details are given in Table A1. The stroke for the compressor and expander is the same as for the combustor at 158 mm.

A charge air cooler (CAC) and a low-pressure (LP) accumulator tank are installed between the compressor exhaust and combustor inlet ports. A high-pressure (HP) accumulator tank and an oxidation catalyst are installed between the combustor exhaust and expander intake ports. The oxidation catalyst would eliminate the potential H_2 slip from the combustor, and thus providing additional enthalpy to be converted to work by the expander unit. The catalyst could also be directly incorporated into the HP tank, but for the current simulations, it is assumed to be just upstream due to the model limitations. The combustor exhaust temperatures are also higher than in conventional heavy-duty engines, consistently reaching around 900 °C, thus allowing the use of cheaper catalytic converters with high effectiveness [33,40].

The LP and HP tanks have a volume of 32.4 L each, which is large enough to dampen large pressure fluctuations in the system. Section 3 will provide the details of the 1D model used to simulate the DCEE system.

3. DCEE system 1D model description

The entire DCEE system in this work is modeled in 1D using the GT-Power engine simulation software [41]. The layout of the model is presented in Fig. 1. Each cylinder is represented by an engine cylinder object. However, the combustor unit is modeled differently compared to the compressor and expander. It includes a combustion object, which imposes precalculated heat release rate and fraction of fuel burned (combustion efficiency). These are taken from the 3D CFD simulations of H_2 combustion, which are described in more detail in Section 4. The heat transfer and friction loss modeling are described in Sections 3.1 and 3.2, respectively. The results of the 1D GT simulations of the combustion cylinder were calibrated against the 3D CFD data, as described in Section 3.3.

3.1. Heat transfer modeling

3.1.1. Heat transfer correlations

Heat transfer in all connecting pipes and ports is modeled using the Colburn correlation [42,43], which is known to be accurate for a fully developed turbulent flow in a conduit. Convective heat transfer in the cylinders is modeled using the Woschni correlation [41,44], which is the most commonly used model for 0D/1D simulations. In accordance with [44], the radiation heat transfer is assumed to be proportional to the burning rate, hence is lumped into the convection equation.

3.1.2. Heat transfer multipliers

A heat transfer multiplier (HTM), which appears as a factor in the convective heat transfer coefficient equation, is commonly used to fit the 1D simulation results to more reliable 3D CFD and experimental data. In this work, the HTM for the *combustion cylinder* is chosen based on the results of diesel engine experimental data and high-fidelity 3D CFD simulations of hydrogen combustion. The fitted HTMs vary for different cases and are given in Table A2. The HTM for the combustor intake ports is set at 1.5, while the exhaust ports are assumed to be insulated with ceramic inserts (HTM = 0.1). For the *compressor* and *expander* units, the cylinder HTM is assumed to equal 1.0 in the uninsulated cases, and 0.1 in the insulated ones. For the connecting pipes, the HTM is set at zero, assuming their effective insulation.

3.1.3. Wall temperatures

The wall temperature for the *combustion cylinder* is set at 527, 467, and 337 °C for piston, head, and liner, respectively. These values were deduced from the diesel engine experimental data and are the same in the 3D CFD simulations. The assumption of unchanged wall temperatures between the diesel and different versions of CI H_2 concept is justified by the fact that the wall temperatures can be controlled by adjusting the coolant flow as to keep them at the highest structurally permissible values. For example, if wall heat flux is lower with a certain concept, the coolant flow would also be reduced to stabilize the temperatures at a higher point. This is done to limit heat transfer and improve engine efficiency. The piston temperature for the *compressor* unit is set at 87 °C – the same as for the oil, while the liner and head temperatures are set at the cooling water temperature of 82 °C. For the *expander* unit, owing to its higher operating temperatures compared to the compressor unit, the wall temperatures are calculated using a finite-element solver available in the GT-Power software [41], which takes into account the materials and shape of the cylinder-piston-head assembly, as well as the adjacent valves and ports.

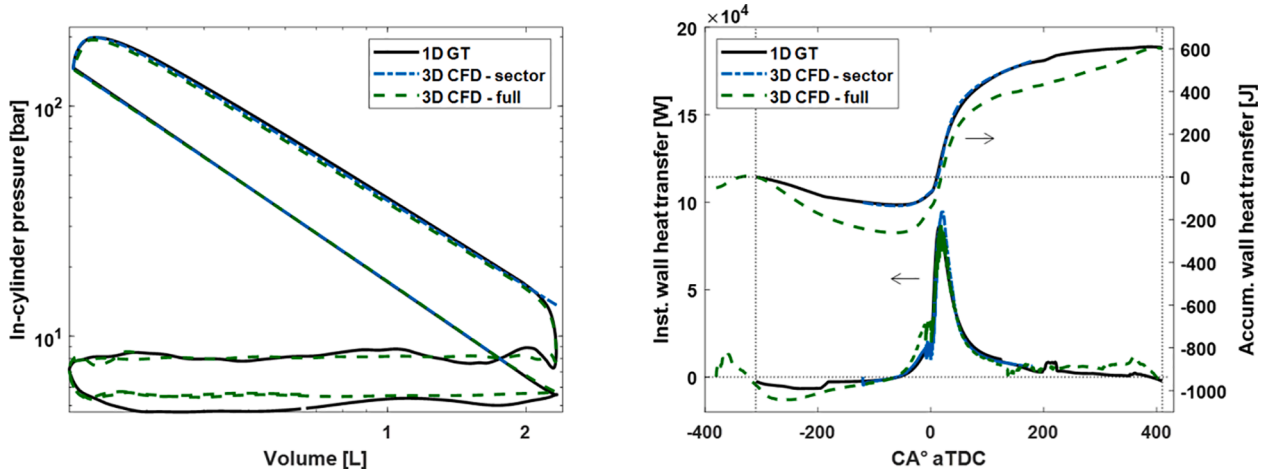

Fig. 2. Combustor unit in-cylinder pressure (left) and accumulated heat transfer (right) to all cylinder walls (including valves) for the 1D GT-Power and 3D Converge CFD models of Case 1.

3.2. Friction loss estimation

Friction mean effective pressure (FMEP) – a nondimensionalized estimate of the friction losses – is modeled in this work using a simple correlation taken from [36] and given in Eqn. (1).

$$FMEP = C_{fr}{*}PCP \quad (1)$$

where PCP is the peak cylinder pressure and C_{fr} is the correlation coefficient equal to 0.006. The choice of this modelling approach is justified in [33,36], and its appropriateness is validated by comparing the results of the FMEP estimations with the experimentally measured data available in the literature [45–50] for medium- and heavy-duty CI engines operating at high load, high-pressure (≈200 bar), and low speed (1200 RPM) conditions. Engine speed was not included in the correlation because it was kept equal in all simulated cases.

3.3. Combustion cylinder 1D model calibration

The 1D GT model of the combustion cylinder of the DCEE was calibrated against the experimentally validated high-fidelity 3D CFD simulation results. Both closed-cycle sector geometry and open-cycle full geometry 3D simulations were used. The sector geometry validation is presented in Section 5. The 1D GT model calibration is carried out by adjusting the displacement of the compressor and expander units, the CAC cooling load, the IVC timing of the expander, and the combustor unit wall HTM in the different parts of the cycle individually (see Table A2). The following metrics were used to achieve the fit:

1. Heat release rate and in-cylinder pressure
2. In-cylinder temperature
3. In-cylinder trapped mass
4. Global equivalence ratio
5. Wall heat transfer in the closed and open parts of the cycle

For more details on the model calibration, refer to [33], where a similar calibration work was performed by the authors. Section 4 will now zoom in on the combustor unit of the DCEE, which was modeled using 3D CFD simulations with the boundary conditions from the 1D model.

4. Combustion cylinder 3D model description

The combustion cylinder of the DCEE in this work is modeled utilizing high-fidelity 3D CFD simulations carried out using the CONVERGE CFD solver [51], version 3.0.13. The numerical setup is largely based on our previous works [22–24,33], which demonstrated its computational efficiency, grid independence, and validity with respect to experimental results from constant-volume chamber and all-metal engine tests.

Simulations of both cylinder sector and full cylinder geometry with valves and ports were carried out. The full-geometry simulations were used to assess the applicability of the sector assumptions (see Section 5), while the sector simulations, owing to their computational efficiency, were used to predict the effects of the proposed system modifications. To model the high-pressure direct H_2 injections, the nozzle inner volume of an HPDI natural gas injector [52] is included in the computational domain. The injection process was validated in [22].

A structured cut-cell Cartesian mesh with a base cell size of $2 \times 2 \times 2$ mm and adaptive mesh refinement (AMR) of scale 3 (down to 0.25 mm) is applied to the cylinder region. The refinement criteria are velocity, temperature, and H_2 species mass fraction to capture the effects of hydrogen's high diffusivity. Additional AMR of scale 4 is applied to cylinder walls to accurately model heat transfer. The intake and exhaust port regions have a base cell size of 4 mm with the AMR of scale 3 (down to 0.5 mm). Additional mesh embeddings of 0.25 mm are applied to the intake and exhaust valve angles – the parts of the valves that are in contact with the valve seats. Also, mesh embeddings of 0.25 mm are applied immediately downstream of the nozzle orifices to ensure that the initial phase of the jet development is captured. The total number of cells in the domain reaches around 1 million in the sector and 10 million in the full geometry simulations.

For turbulence modeling, an RNG k-ε model is used with standard coefficients. The Redlich-Kwong-Soave (RKS) equation of state is adopted with species-specific critical conditions and acentric factors. The species diffusion calculations include the mixture-average binary diffusion assumption. The H_2 combustion is modeled using the SAGE detailed chemistry solver with a detailed kinetic mechanism of H_2 oxidation at high temperatures and pressures (Burke et al. [53]). A

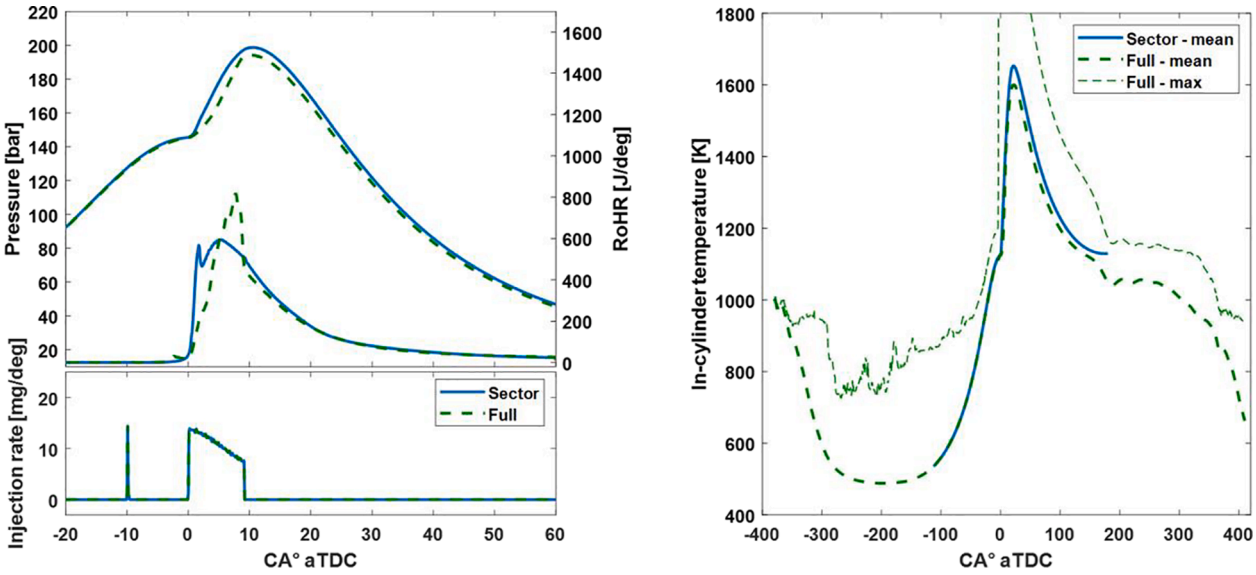

Fig. 3. Injection rate, in-cylinder pressure, and rate of heat release (left), and in-cylinder mean and maximum temperature (right) for the sector- and full-geometry 3D Converge CFD simulations of Case 1.

variable time-step algorithm is utilized for time integration with the CFL limits of 0.3, 2.0, and 50.0 for convection, diffusion, and Mach phenomena, respectively.

Section 5 will now discuss the sector geometry modeling in comparison to the full geometry modeling and justify the use of the former for the purposes of this study.

5. Validation of the sector- against full-geometry modeling

The first step in the research approach is to answer the question of the applicability of the sector modeling approach, especially with regards to the effects of the real gas exchange process as opposed to the homogeneous quiescent charge assumption with the sector. In this section, a full engine geometry simulation with gas exchange and combustion is analyzed and compared to the sector simulation.

Figure 2 (left) shows that the exhaust stroke is captured very well by the GT-Power model. Considering this, the deviations during the intake stroke between the 3D CFD and 1D GT models are likely due to the acoustic effects (pressure waves) captured by the latter in the presence of the compressor and the LP tank, while the former assumes a constant pressure on the intake. The lack of acoustic effects in the 3D CFD case was compensated by adjusting the inflow boundary pressure to match the in-cylinder pressure in the GT case at IVC.

5.1. Wall heat transfer during gas exchange

Another important factor that the full geometry simulation can shed light to is the heat transfer to the cylinder walls during gas exchange. Fig. 2 (right) shows that in the closed-cycle part, the heat transfer in 1D GT model matches exactly with the 3D CFD sector simulation, which is expected considering that the 1D model has already been calibrated. However, the full-geometry simulation shows a higher wall heat transfer rate during the gas exchange, both in the intake and exhaust strokes. Most of the difference is caused by the heat transfer to the valves, which is not captured well by the 1D model. Attempting to match the valve heat transfer would require a very large adjustments to the HTMs, which are normally not recommended.

On the other hand, despite the discrepancies described above, the final accumulated loss of heat to the walls over the entire cycle in 1D model matches well with the 3D model. This is firstly because the valve heat transfer still represents a small proportion of the total wall heat transfer, which instead is dominated by the piston, head, and liner shortly after the TDC (as seen in Fig. 2, these are well matched). Secondly, the larger heat transfer to the walls during the exhaust stroke is compensated by the larger heat transfer *from the walls* to the in-cylinder gas during the intake. Thus, it is concluded that the HTMs chosen based on the sector geometry provide a satisfactory match between the 3D Converge CFD and 1D GT-Power simulation results.

5.2. Ignition and combustion

Figure 3 (left) compares the heat release and pressure traces of the full-geometry open-cycle 3D CFD simulation and the corresponding sector simulation. Some notable differences are clearly observed: the heat release rate in the former is initially lower, but later, closer to the CA50, becomes higher. This is explained in the following.

First, the ignition and combustion of some of the H_2 jets in the full-geometry case are delayed. This is caused by a slightly heterogeneous distribution of temperature in the cylinder with the actual gas exchange process modeled. This is illustrated in Fig. 4, where the intake-port side of the cylinder clearly exhibits lower temperature 10 CA° before TDC, which is explained by the colder intake air displacing the hotter residuals from the intake side toward the exhaust side of the cylinder. As a result, the pilot plumes on the intake side did not ignite on time, which led to a delayed ignition and combustion of several main jets, as shown in Fig. 4 (bottom).

Because the sector simulations do not cover the gas exchange process, there are no regions with significantly colder intake gas, and thus all pilot plumes ignite at the same time. Note that, in the full-geometry simulation, due to the delayed ignition of some of the jets, premixed combustion accounts for a larger proportion of heat release, thus briefly leading to a higher peak in the RoHR trace. Another factor that led to a generally lower heat release rate during the injection process in the full-geometry case is the closer proximity of the piston to the injector nozzle, and hence, less space for the jet development and more jet-piston interactions compared to the sector case. The TDC position of the piston is

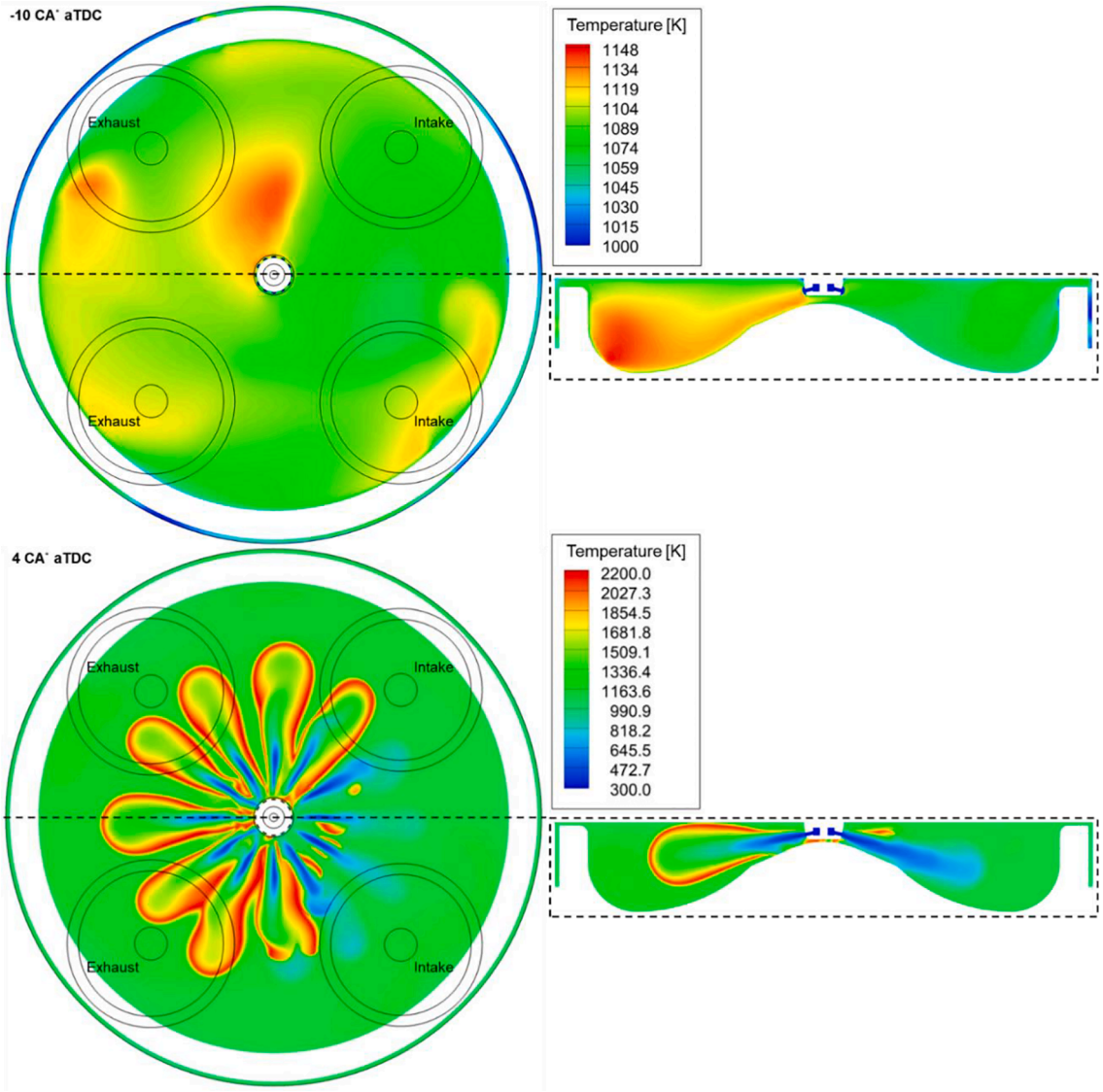

Fig. 4. Cylinder temperature slices for the full-geometry 3D Converge CFD simulation of Case 1. Note the difference in the range of the two colorbars.

higher with the full engine geometry due to the more complex shape of the cylinder head, and especially the valve seat recesses, which add more dead volume to the cylinder, and hence must be compensated by the piston position to attain the same compression ratio.

These results, first, suggest that the minimum target temperature that was chosen based on the sector simulations might not be high enough in an actual engine due to a certain level of heterogeneity of the trapped charge. Approximately 50 K higher TDC temperature might be required for reliable ignition. On the other hand, the more optimized versions of the DCEE with removed CAC are not expected to exhibit these issues because the peak cylinder temperatures before fuel injection would be above 1250 K, far beyond the ignition point of H_2 (Section 7.2 onward).

The above results also suggest that, when optimizing the piston shape for the jet mixing dominated combustion, a greater care must be given to the dead volumes, such as valve recesses, even at the CR as low as 11.5:1. Considering that combustion in this concept is non-premixed and the reacting jets are never in contact with the piston crevices, the dead volumes may be compensated in the sector simulations by adopting artificially deep crevices.

5.3. *Post-combustion during exhaust stroke*

Fig. 3 (right) shows that the gas temperature in the full-geometry case during the exhaust stroke can locally be approximately 100 K higher than the average, and reaches around 1150 K, which is generally high-enough for H_2 ignition. Thus, it is possible that the remaining H_2 that did not mix with O_2 during the expansion stroke may eventually mix and burn during the exhaust stroke, likely in the exhaust ports, as long as the global λ is above 1. For cases with higher exhaust temperatures, i.e., non-intercooled and high-pressure cases, the post-combustion of H_2 in the exhaust ports is even more likely. This suggests that the catalytic burner incorporated in the HP tank of the DCEE might not be necessary. However, considering the limitations of the 1D model, the burner was

Table 1
Names of the different cases, their purpose, fixed and changed parameters, and the cases they are compared to. The red frame around a parameter in the third column indicates that it was changed compared to the case indicated in the fourth column. All the parameters that are not highlighted are fixed.

Case name	*Investigation of the effects of …*	*Changed and fixed parameters*	*Compared to …*
Case 1	The reference case		
Case 2	Implementation of a catalytic burner	B_{compr} CR **λ** PCP B_{exp} HTMs T_{in} η_{comb} Int_{exp} m_f PMP	Case 1
Case 3	Removal of the intercooling at fixed PMP	**B_{compr}** CR λ PCP B_{exp} HTMs **T_{in}** η_{comb} Int_{exp} **m_f** PMP	Case 2
Case 4	Removal of the intercooling at fixed compressor size	B_{compr} CR λ **PCP** B_{exp} HTMs **T_{in}** η_{comb} Int_{exp} m_f **PMP**	Case 2
Case 5	Insulation of the expander at fixed PMP	**B_{compr}** CR λ PCP B_{exp} HTMs T_{in} η_{comb} Int_{exp} **m_f** PMP	Case 3
Case 6	Insulation of the expander at fixed compressor size	B_{compr} CR **λ** PCP B_{exp} HTMs T_{in} η_{comb} Int_{exp} m_f PMP	Case 4
Case 7	Condensation of water in the EGR cooler at fixed PMP	**B_{compr}** CR **λ** PCP B_{exp} HTMs **T_{in}** η_{comb} Int_{exp} **m_f** PMP	Case 5
Case 8	Condensation of water in the EGR cooler at fixed compressor size	B_{compr} CR λ **PCP** B_{exp} HTMs **T_{in}** η_{comb} Int_{exp} **m_f** **PMP**	Case 6
Case 9	Shifted LP/HP crossover point at fixed PMP	**B_{compr}** CR λ **PCP** B_{exp} HTMs T_{in} η_{comb} **Int_{exp}** **m_f** PMP	Case 7
Case 10	Shifted LP/HP crossover point at fixed compressor size	B_{compr} CR λ **PCP** B_{exp} HTMs **T_{in}** η_{comb} **Int_{exp}** **m_f** **PMP**	Case 8
Case 11	Combustion efficiency versus engine load	**B_{compr}** CR **λ** **PCP** B_{exp} HTMs T_{in} **η_{comb}** Int_{exp} **m_f** PMP	Case 8
Case 12	Higher combustor pressure and load at fixed lambda (1.16) – Boosted LP side	**B_{compr}** CR λ **PCP** **B_{exp}** **HTMs** **T_{in}** **η_{comb}** Int_{exp} **m_f** **PMP**	Case 10
Case 13	Higher combustor pressure and load at higher lambda (1.36) – Boosted LP side	**B_{compr}** CR **λ** PCP B_{exp} **HTMs** T_{in} **η_{comb}** Int_{exp} **m_f** **PMP**	Case 12
Case 14	Higher combustor pressure at higher lambda (1.67) – Boosted LP side	**B_{compr}** CR **λ** PCP B_{exp} HTMs **T_{in}** **η_{comb}** Int_{exp} **m_f** **PMP**	Case 13
Case 15	Higher combustor pressure – increased CR of the HP side	**B_{compr}** **CR** λ PCP **B_{exp}** HTMs **T_{in}** η_{comb} Int_{exp} **m_f** **PMP**	Case 13
Case 16	Reintroduction of the intercooling at higher pressures at fixed PCPs	**B_{compr}** CR **λ** PCP B_{exp} HTMs **T_{in}** η_{comb} Int_{exp} **m_f** PMP	Case 13

B_{compr} = compressor bore
B_{exp} = expander bore
Int_{exp} = expander intake valve event duration
CR = combustor compression ratio
HTMs = combustor wall heat transfer multipliers
m_f = injected fuel mass
λ = air-fuel equivalence ratio
T_{in} = combustor intake gas temperature
PMP = peak motoring pressure
PCP = peak cylinder pressure (after combustion)
η_{comb} = combustion efficiency

kept ensuring complete combustion.

With all the important modeling details now discussed, the following Section 6 will describe the research approach taken in this work with details on the parametric cases simulated.

6. Parametric study cases

This section elaborates on the parametric studies performed in this work. The goal is to achieve the maximum system brake thermal efficiency, while taking into account the practical limitations of the DCEE concept and its base engine (Volvo D13). These limitations include the bore of the combustor unit, the stroke of the combustor, compressor and expander units, the peak cylinder pressures, combustor intake and exhaust temperatures, etc. [36] A total of 17 different cases are compared; each one is designed to investigate the effects of different modifications to the system. The case names, objectives, as well as the fixed and varied parameters are summarized in Table 1. Some notable modifications include: Case 2 – implementation of a catalytic burner in the combustor exhaust to reduce/eliminate unburned fuel and provide extra enthalpy for the expander unit; Case 3 and 4 – removal of the intercooling after the compressor to reduce the heat losses and provide more heat for H_2 ignition; Case 5 and 6 – insulation of the expander unit to reduce heat losses; Case 7 and 8 – condensation and removal of water from the EGR cooler to increase the specific heat ratio (γ) and improve the cycle thermodynamic efficiency; Case 9 and 10 – raising/lowering the LP/HP crossover point to find an optimum allocation of work between the LP and HP sides of the system; Case 11 – finding a favorable tradeoff between combustion efficiency and engine load in terms of global equivalence ratio (λ); Case 12, 13, and 14 – further boosting of the combustor unit up to a PCP of 300 bar at different λ to further improve the cycle thermodynamic efficiency and find an optimum λ; Case 15 – increase in the CR of the combustor unit as the alternative strategy to the previous for improved thermodynamics; Case 16 – reintroducing the intercooling to find out whether the low-pressure heat loss tradeoffs still persist at the PCP of 300 bar. Note that the LP/HP crossover point is the pressure at which the exhaust gas from the combustor is passed into the HP tank and the expander unit. Many parametric cases are studied in pairs, with a fixed compressor size and a fixed peak motoring pressure (PMP – before combustion). These are the two optimization alternatives, where the former case is generally more applicable when the pressures are not near 300 bar (dictated by the structural limitations), while the latter becomes more relevant in the vicinity of the maximum pressure

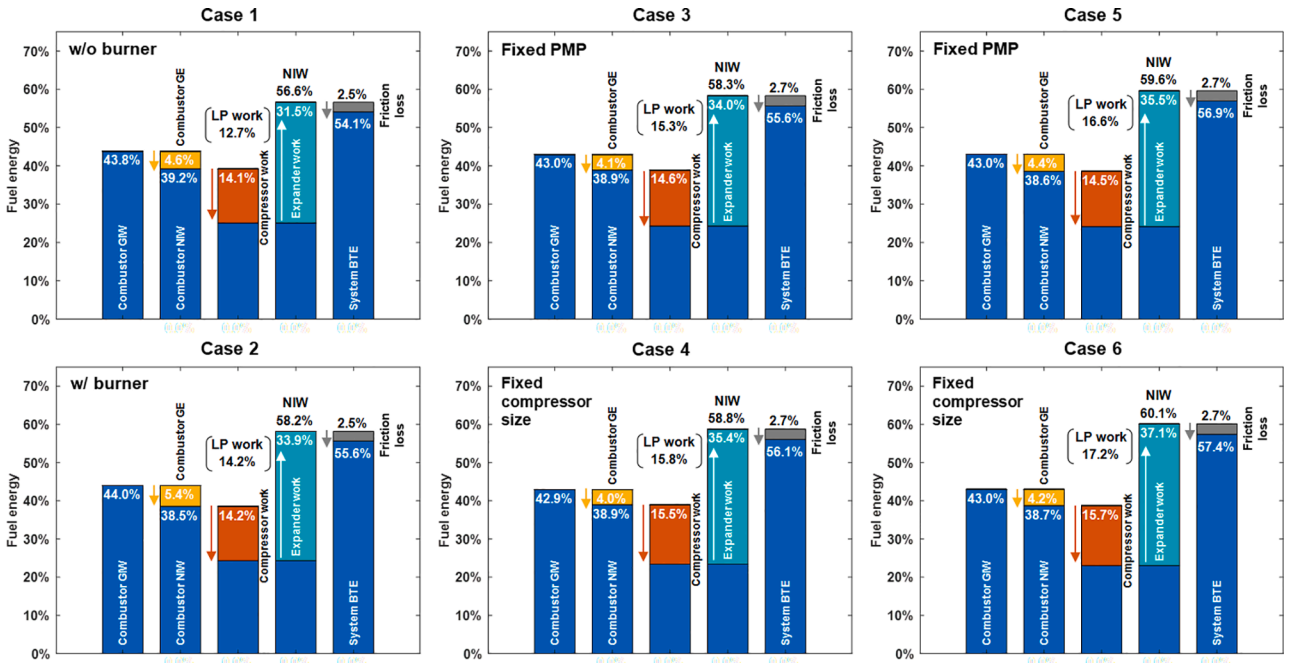

Fig. 5. Different components of the DCEE system energy flow for Cases 1–6. PMP stands for peak motoring pressure.

limits. For details on the engine specifications and operating conditions, refer to Tables A1 to A3 in the Appendix.

- In Appendix B3. DCEE fueled by hydrogen versus diesel, the best H_2 DCEE configuration is also compared to the diesel-fueled variant to show the potential of the H_2 fuel against the current state of the art.

With all parametric cases defined, Section 7 will now present and discuss the results of the study.

7. Results and discussion

Many results in this section are presented in the form of energy flow bar charts, such as those presented in Fig. 5. These show how much of the fuel energy entering the combustor unit is converted into the gross indicated work (GIW) on the piston, how much of it is then lost to the gas exchange (GE) losses in the combustor unit, how much was needed to compress the air for combustor boosting, and how much of the compression and combustion energy is then recovered by the expander unit. The net work produced by the low-pressure (LP) part of the system is then defined according to Eqn. (2).

$$\mathrm{LP_{work}} = \mathrm{NIW_{compr}} + \mathrm{NIW_{expan}} + \mathrm{GEW_{comb}} \tag{2}$$

where $\mathrm{LP_{work}}$ is work produced in the low-pressure part of the system, $\mathrm{NIW_{compr}}$ is compressor net indicated work (negative), $\mathrm{NIW_{expan}}$ is expander net indicated work (positive), and $\mathrm{GEW_{comb}}$ is combustor gas exchange work (negative). Note that the combustor pumping losses are included in the definition of the LP work. This is because combustor pumping is largely a function of the low-pressure part of the cycle.

Finally, after considering the HP and LP indicated piston work, the chart presents the net indicated system work (NIW), from which the friction (+parasitic) losses are subtracted to arrive at the system brake thermal efficiency (BTE).

7.1. Addition of a burner (Case 2, 3D CFD)

The first step to improve system BTE is to recuperate some of the incomplete combustion losses from the combustor unit by using a catalytic burner in the HP tank. The results of this modifications are presented in Fig. 5, first column. The total system BTE increased by 1.5%-points, which means that approximately half of the incomplete combustion losses are recouped in the LP part of the system (see "Combustion efficiency" in Table A3). In the presence of the burner, the combustor lambda reduced from 1.20 to 1.15 due to the smaller oxygen concentration in the residual and EGR gases. However, it proved to be inconsequential for the final efficiency.

7.2. Removal of the intercooling (Cases 3 and 4)

The removal of the intercooling, depending on how it is done, may improve the system BTE. When the combustor PMP is fixed at around 150 bar (Case 3 in Fig. 5), the removal of the intercooling has no effect on the BTE. In this case, as the intake temperature is raised, the air mass trapped in the combustion cylinder reduces, and to keep constant lambda, the fueling must also be reduced. This leads to a lower combustor GIW. On the other hand, less energy is lost in the LP part of the cycle as the CAC loss and compressor negative work reduce. This results in a higher LP work, which compensates for the lost HP work. As a result, the system BTE stays unchanged.

Instead of maintaining constant PMP, if the compressor size is kept unchanged compared to Case 1 and Case 2, the system sees a 0.5%-point BTE increase in Case 4 (see Fig. 5, second column). In this case, the combustor performance is still slightly compromised but the entire LP part of the cycle produces significantly more work. Because the overall mass flow rate through the entire system and amount of fuel injected is now back at the Case 2 levels, but the CAC losses are now eliminated, more energy is transferred to the expander unit and put to effective use.

It is evident that, to claim the efficiency benefits with Case 4 having eliminated intercooling, the reduction in the intake gas density must be compensated for by higher pressure levels (at the same geometrical CR and displacements). The removal of the intercooling in Case 4 leads to a 10% increase in the PMP through a higher combustor inlet pressure but causes no alteration in lambda. This is because the combustor-trapped mass did not increase (compared to Case 2), as the increase in pressure was not due to the higher mass flow rate but due to the increased inlet temperature (consider the ideal gas law). This also caused a higher combustor wall heat transfer but was overall compensated for by the expander positive work.

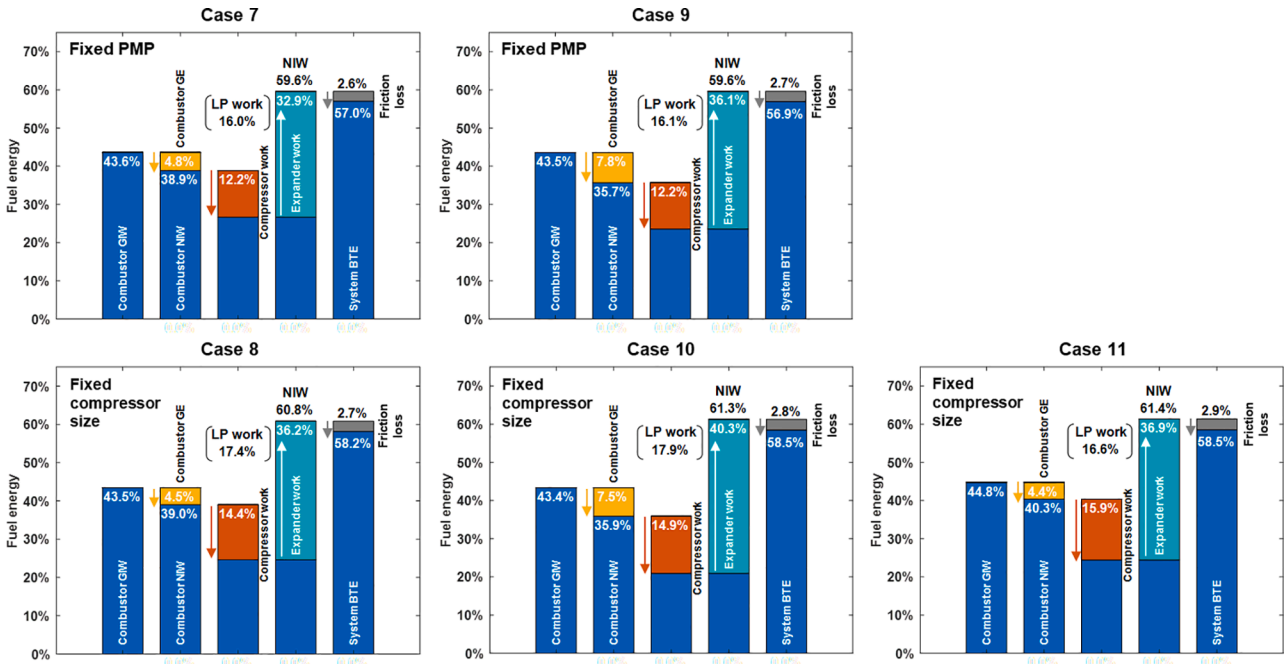

Fig. 6. Different components of the DCEE system energy flow for Cases 7–11. PMP stands for peak motoring pressure.

As such, we also see a tradeoff between the better thermodynamics of the combustor unit compared to the expander (higher temperatures), and larger wall heat losses at the higher temperatures.

7.3. Insulation of the expander (Cases 5 and 6)

Insulation of the expander with the convective heat transfer multiplier of 0.1 led to a 1.3% increase in the system BTE both for the case with a fixed combustor PMP and fixed compressor size (see Fig. 5, third column). The effects of this change are more unidimensional. A very large reduction in the expander heat transfer loss is observed, in the range of 3% of the total fuel energy. Some of the saved work is then lost to the expander exhaust, but most of it is put to effective use. The improvements are attributed to the LP part of the system. The tradeoff between the thermodynamics and the wall heat losses also shifted more favorably toward the LP side as the expander is well insulated. Note that the compressor unit could also be insulated; however, this was previously shown to yield insignificant efficiency improvements due to the extremely low heat loss in the compressor compared to other components of the system (for details, refer to [33]).

7.4. Water condensation in the EGR cooler (Cases 7 and 8)

A limitation of the previous models is that no condensation of water was modeled in the EGR cooler, even though the temperature reduced from 600 to 700 K down to almost ambient. In this subsection, the water condensation in the EGR cooler is taken into account, and its effects are discussed. In Case 7, out of approximately 13.7% water content by mass in the expander exhaust, over 90% is condensed out and removed in the EGR loop. As a result, more air, with a higher specific heat ratio (γ), is drawn in and compressed by the compressor unit.

In Case 7, to maintain a PMP of 150 bar, the compressor size had to be reduced even compared to Case 5 in order to account for the higher γ. The total mass flow rate though the system (hence, combustor trapped mass) reduced. However, because the water in the intake is substituted with air, λ is not affected, and the fueling remained the same (as in Case 5). As shown in Fig. 6, the resultant system BTE in Case 7 did not change significantly compared to Case 5 with the PMP fixed at 150 bar. Comparatively more work is produced in the HP part (combustor) because the difference in γ is compensated by the smaller LP part of the system, which also produced less work as a result.

On the other hand, if the compressor size is kept the same as in Case 5 (or 3,2, and 1), the system BTE sees a 0.8%-point increase in Case 8. This is achieved largely via a higher combustor work (HP part of the system). The combustor GIW increased due to the higher pressure and temperature levels caused by a higher γ, as well as due to a higher fueling. However, the heat transfer losses in the combustor also increased, even though the resultant GIW is still higher than before.

It may also be argued that, previously, the total DCEE efficiency and the proportion of work produced in the HP part were underpredicted for the chosen total engine displacement, because with the updated model (that considers water condensation), the compressor size is significantly smaller.

7.5. Shifted LP/HP crossover point (Cases 9 and 10)

To investigate the effect of the combustor exhaust / expander intake crossover point, the expander inlet valve event duration is reduced, thus increasing the resistance, and raising the pressure, and consequently, the crossover point. This is done, again at either fixed PMP or fixed compressor size, and the results are presented in Fig. 6 (second column).

At fixed PMP (Case 9), the raised crossover point does not affect the BTE significantly. The system energy distribution stays largely unchanged; only the combustor pumping work is transformed into work on the expander piston. The HP tank temperature was not affected significantly either, because the risen pressure is compensated by the lower load. Overall, it is seen that shorter expander intake event, and thus higher crossover point, is not worthwhile pursuing when the PMPs are limited.

On the other hand, when the compressor displacement is kept constant, the HP tank and expander inlet pressures increased from 9.1 bar (Case 8) to 11.5 bar (Case 10). As a result, the system BTE increased by 0.3% points. The improvement comes from the LP part of the cycle, which sees a 0.5%-point increase in the useful work, while the combustor performance stayed largely unchanged.

Important factor enabling the improvement is the combustor's relatively low heat transfer loss during the gas exchange, which does not put a prohibitively high price on the higher crossover point. This is

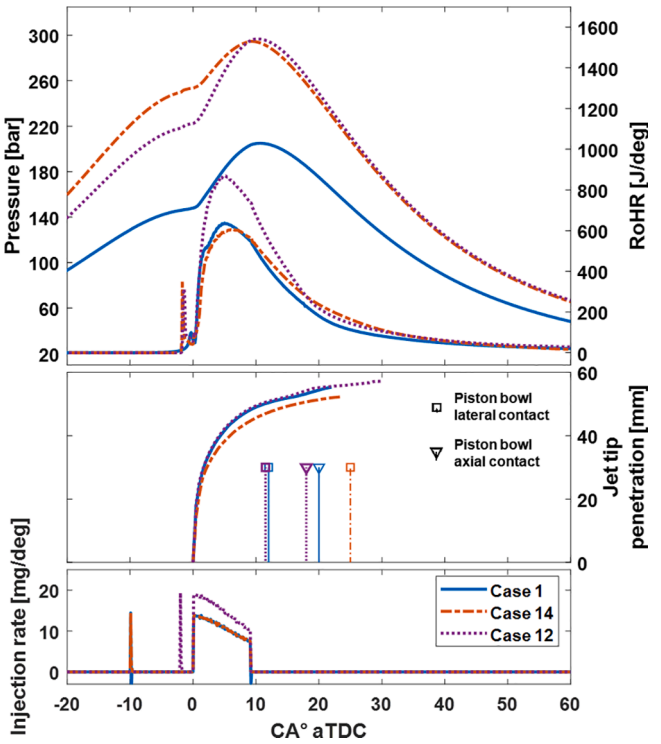

Fig. 7. Injection rate, jet tip penetration and jet-piston collision timing, rate of heat release, and in-cylinder (combustor) pressure trace for Cases 1, 14, and 12.

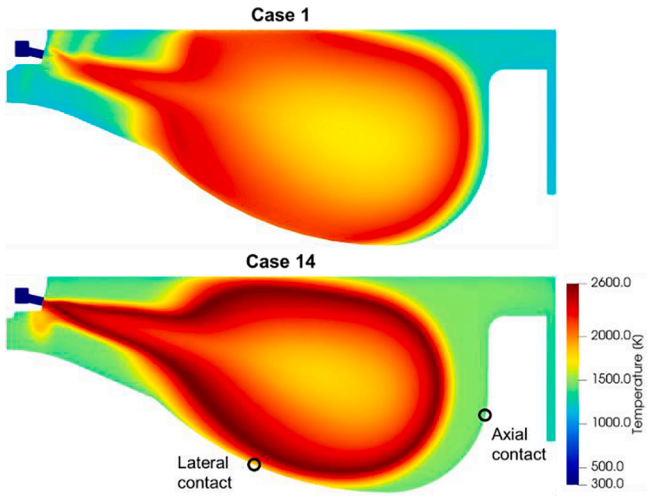

Fig. 8. Vertical temperature slices at the jet center for Case 1 and Case 14. The lateral and axial contact locations are to be used in conjunction with Fig. 7.

because the combustor's exhaust ports are insulated with ceramic inserts. Additionally, as mentioned previously, the low heat losses in the expander make the system efficiency to favor the higher crossover point. However, the higher crossover point also causes elevated HP tank temperatures, thus it might be more worthwhile from a practical standpoint to shift the HP-LP work balance toward the former to limit HP tank temperatures and make the design of the valve system simpler.

Note that the combustor work did not significantly decrease because the combustor's intake pressure was allowed to increase with the higher expander crossover point, thus increasing the system effective compression ratio, which ultimately enabled the higher efficiency.

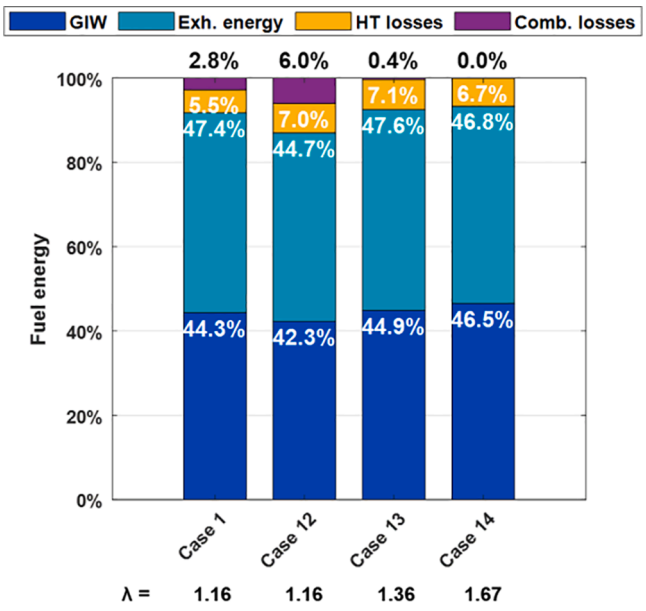

Fig. 9. Fuel energy distribution between the gross indicated work (GIW), exhaust energy, heat transfer (HT) and incomplete combustion losses for the combustion cylinder of the DCEE at a PCP of 300 bar and different air excess ratios.

7.6. Combustion efficiency versus load (Case 11)

In Case 11, the global λ was increased to ~ 1.4 by injecting less fuel. This is expected to reduce the percentage of unburned fuel in the combustor down to only 0.1%, considering the results of the CFD simulations presented in Section 7.7.2. This case is now compared to Case 8 to assess the importance of a higher combustion efficiency compared to a higher engine load.

From Fig. 6, it is seen that the combustor GIW in Case 11 increased by 1.3%-points, while the LP work reduced by 0.8%-points. This, together with a slightly higher percentage of friction loss caused by the lower engine load, leads to only 0.3%-point improvement in the system BTE. The higher efficiency can be explained by the better thermodynamics associated with the heat addition at higher temperatures in the combustor, as opposed to that at lower temperatures in the catalytic burner (LP part).

Another important difference is the HP tank temperatures, which are approximately 80°lower in Case 11 with the higher combustion efficiency compared to Case 8. Thus, it is also better from the practical standpoint to maximize combustion efficiency at the expense of the engine load. Note that the engine brake power in Case 11 reduced by 10% compared to Case 8 ($P_{brake,\ Case\ 11} = 70.9$ kW versus $P_{brake,\ Case\ 8} = 79.0$ kW for the single-combustor configuration of the DCEE).

7.7. Effects of a higher operating pressure on the hydrogen combustion cycle (boosted LP side)

To further improve the engine efficiency, the maximum combustion cylinder pressures can be increased, reaching 300 bar. This is the Volvo D13 engine's reported pressure limit. The PCPs can be increased in two ways, by modifying the LP side or the HP side. The operating pressures of the HP side (the combustor unit) can only be increased by installing a piston with a higher CR; other means, such as changing the displacement of the unit, would necessitate costly modifications or a complete redesign of the base engine. Alternatively, the PCPs can be increased via the LP side by implementing a larger compressor and expander units. The latter option is investigated using 3D and 1D CFD simulations and discussed in this subsection. The alternative scenario with the increased

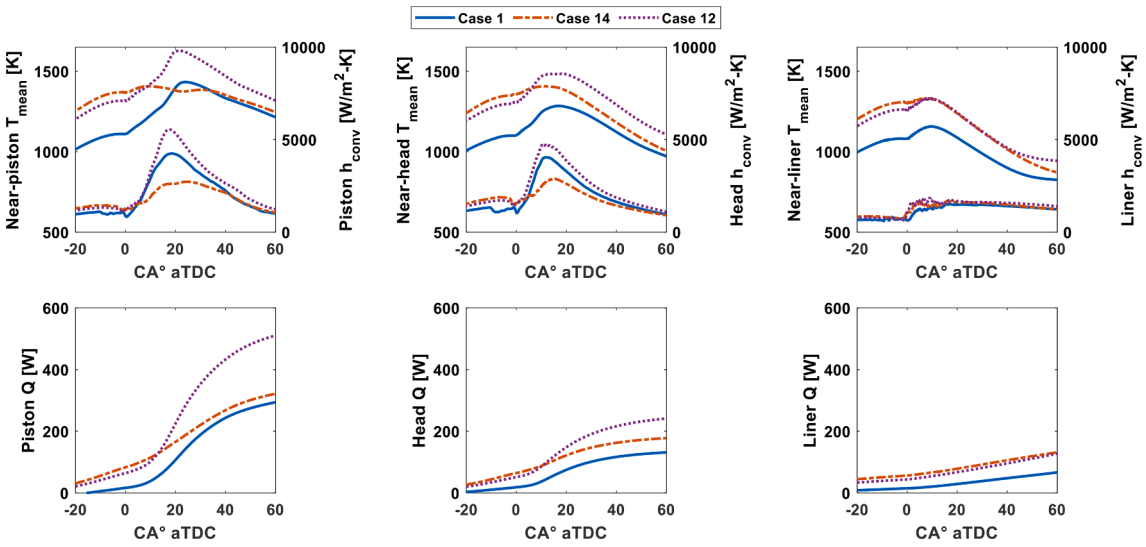

Fig. 10. Mean temperature, convection heat transfer coefficient, and total heat loss as a function of crank angle for piston, head, and liner of the combustion cylinder of the DCEE.

Table 2
Combustion cylinder intake air composition and EGR specific heat ratio for Cases 1 and 12.

	Case 1	Case 12
$Y_{O2,\ int}$	0.1311	0.1229
$Y_{N2,\ int}$	0.7580	0.8534
$Y_{H2O,\ int}$	0.1109	0.0237
γ_{EGR}	1.3778	1.3961

combustor CR is explored in Appendix B1. DCEE system at higher pressure (increased CR of the HP side).

7.7.1. Hydrogen jet dynamics

Case 1 vs Case 14.

Fig. 7 shows that Case 14 with a boosted intake and maintained injection rate has a lower heat release rate compared to the low-pressure alternative, Case 1. This is explained by the slower jet penetration and plume radial dispersion or growth in the former. These are deduced from the jet tip penetration and piston contact timing shown in Fig. 7. The lateral and axial contact definitions are further clarified in Fig. 8.

The slowed jet penetration and growth are caused by the higher in-cylinder charge density at higher pressures in Case 14, which inflicts a larger resistance on the jet. The charge density at TDC is 56.3 kg/m^3 versus 40.4 kg/m^3 for Case 14 and Case 1, respectively. As also shown in Fig. 8, the resultant reacting plume size is significantly smaller with Case 14, while its temperature is higher (more on that in the following).

Note that, combustion modeling in Case 14 is turned on at −2 CA° aTDC, to coincide with the pilot ignition timing in Case 1. This is done to make sure that an earlier ignition in the former, caused by the higher temperatures, would not affect the comparison.

Case 1 vs Case 12.

The second high-pressure case that is simulated for comparison with Case 1 is Case 12, which has a maintained global λ of 1.16, thus larger amount of injected fuel and higher injection rate. As seen in Fig. 7, the pilot plume ignites in<1 CA° in Case 12, owing to the higher in-cylinder charge temperatures (see combustor inlet T in Table A3). The heat release rate is also expectedly higher due to the larger fuel amount. The main jet penetration and growth in Case 12 are very similar to those for Case 1. This suggests that the higher injection rate, and hence inflow jet momentum, in Case 12 compensates for the larger resistance by the denser in-cylinder charge, yielding similar jet development to Case 1. However, the injection pressure is now approximately 320 bar, which means that the differential pressure between the injector and the cylinder at TDC increased to about 100 bar, as opposed to 70 bar in Case 1.

7.7.2. Thermodynamic losses

Case 1 vs Case 14.

Continuing the comparison between Case 1 (low pressure) and Case 14 (high pressure, same fueling), Fig. 9 shows that the gross indicated efficiency of the combustion cylinder is 2.2%-points higher in the latter case. This is achieved via the reduced incomplete combustion and exhaust losses, which in turn are improved by the larger air excess ratio (λ = 1.67 instead of 1.16) at the same fueling rate.

On the other hand, the heat transfer losses in Case 14 increased by 22%, or 1.2%-points. This increase is explained by the near-wall mean

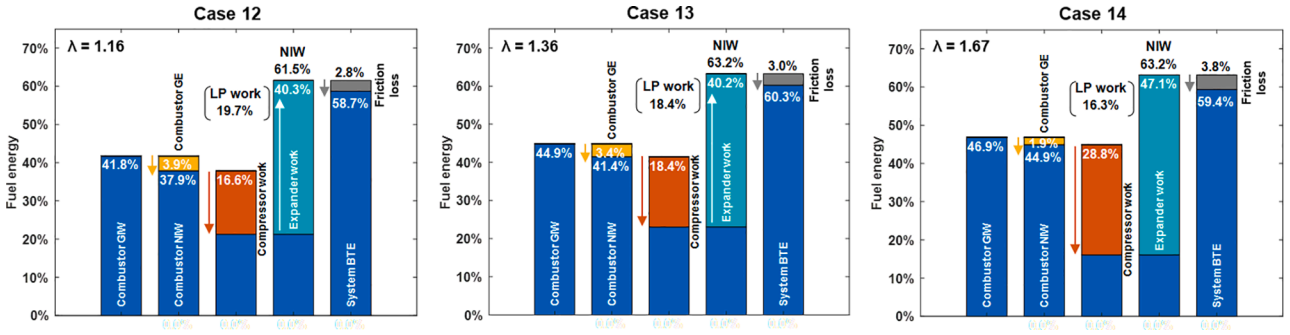

Fig. 11. Different components of the DCEE system energy flow at a PCP of 300 bar with varied air excess ratio and engine load.

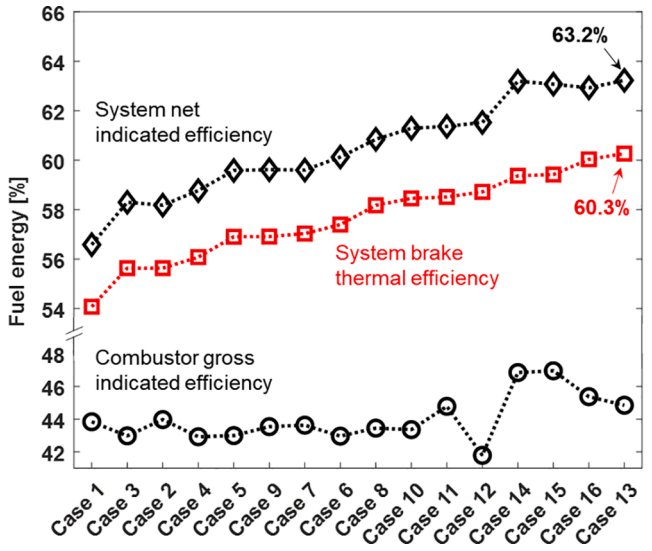

Fig. 12. Progression of the combustor unit gross indicated efficiency, and the DCEE system net indicated and brake thermal efficiency.

temperatures (T_{mean}) and convective heat transfer coefficient (h_{conv}), and accumulated heat transfer (Q) to each cylinder wall presented in Fig. 10. In the expansion stroke, during the injection and combustion, the h_{conv} is significantly lower for Case 14, while the near-wall T_{mean} is generally higher. As a result, after TDC, these two counteracting factors balance each other, giving no appreciable net difference in the expansion stroke heat transfer. However, during the compression stroke, the temperatures in Case 14 are significantly higher, while heat transfer coefficients are approximately equal. As a result, the higher heat transfer losses are attributed to the wall heat loss during the compression stroke.

Case 1 vs Case 12.

Figure 9 shows that the fraction of unburned fuel losses is about twice as high with Case 12 compared to Case 1. Considering that the jet development and global equivalence ratio are almost identical for the two, the reason for the higher losses must be related to the reaction equivalence ratio – essentially the concentration of O_2 in the cylinder. As shown in Table 2, Case 12 exhibits a considerable reduction in the O_2 mass fraction in the combustion cylinder intake gas, which despite the constant air–fuel equivalence ratio, still leads to a lower *reaction* air–fuel equivalence ratio, which is more directly linked to the combustion efficiency. This is caused partly by the implementation of the catalytic burner in the HP tank, which makes the unburned H_2 react with O_2, thus reducing the amount of the latter in the EGR gas. However, this proved to have relatively minor effect compared to the removal of water from the EGR cooler in Case 12. Recall that the water condensation has been modeled starting from Case 7.

The removed H_2O would be substituted by N_2, as the only remaining species, O_2, would be almost completely consumed by the combustion. Since H_2O has significantly lower γ compared to N_2, the EGR gas devoid of H_2O would have higher γ (see Table 2). As a result, the EGR portion of the intake gas in the combustion cylinder of the Case 12 has a higher partial pressure, and hence, a larger contribution to achieving a certain PCP (300 bar in this case). This necessitates a reduction in the overall mass flow rate through the system to maintain a constant volumetric flow rate and PCP, hence less fresh air and lower O_2 concentration.

The wall heat transfer in Case 12 exhibits very similar trends as that in Case 1, as shown in Fig. 10, albeit the values are considerably higher in the former owing to the higher temperatures. The similar trends are explained by the almost identical jet development, as explained in Section 7.7.1. It is also observed in Fig. 10 that the wall heat losses are dominated by the piston heat transfer, followed by the cylinder head, and finally the cylinder liner.

7.7.3. NOx emissions

The potential NOx emissions from the combustor unit of the DCEE are estimated in this work using the extended Zeldovich mechanism. Table A4 shows the results at low (Case 1) and high pressures (Cases 12, 13, and 14). These are only combustor-out emissions which assume no aftertreatment.

Overall, *manageable amounts of NOx are reported*. Note that the performance of the Zeldovich mechanism in hydrogen combustion engines has been questioned in the literature due to the fact that it was formulated for hydrocarbon fuels [54]. Thus, an improved NOx estimation methodology will be attempted in a future study.

7.8. DCEE system at higher pressure and engine load (boosted LP side), 3D CFD supported

Case 12 vs Case 13 vs Case 14.

In the previous sections, when discussing the higher-pressure (300 bar PCP) cases, either the injected fuel amount (Case 14) or the lambda was fixed (Case 12) compared to the lower-pressure Case 1. Case 12 had lower lambda, and hence high incomplete combustion losses but high engine load, while Case 14 had higher lambda, hence almost no incomplete combustion losses, and higher gross indicated efficiency, but lower engine load. It is not obvious from the combustion cylinder analysis alone which scenario would be better for the entire DCEE system, and if there is a better "sweet spot" with respect to the global equivalence ratio selection.

In this section, three cases with different λ's are compared in the context of the entire DCEE system by imposing the 3D CFD simulation results in the 1D GT-Power model of the powertrain. The results are presented in Fig. 11. It was already concluded in Section 7.6 that sacrificing the engine load in favor of improved combustion efficiency may be preferred at lower pressures from the system efficiency and practical standpoints. Likewise, at the PCP of 300 bar, Case 13 with $\lambda = 1.36$ seems to offer the optimum tradeoff between the engine load, and hence mechanical efficiency, and combustion efficiency, achieving a BTE of 60.3%. The lower-λ Case 12 suffers from too low combustion efficiency and shows the lowest system BTE among the three cases. Case 14, on the other hand, shows good thermodynamic efficiency, achieving the NIW as high as Case 13, but the lower engine load results in the larger fraction of fuel energy lost to friction, which reduces the BTE by 0.9%-points compared to Case 13.

Case 13 vs Case 11.

Comparing the high-pressure Case 13 (Fig. 11, middle) with the low-pressure Case 11 (Fig. 6), it is seen that the system BTE is almost 1.8%-points higher in the former, with a 68 bar increase in the PCP. The global λ in the boosted case is approximately equal to that of the low-pressure case, thus the fueling is also higher in the former, which results in only a marginal increase in the proportion of friction losses despite the higher pressures. The combustor gross indicated efficiency is largely unchanged, while the LP work is 1.8%-points higher with Case 13, giving the final efficiency improvement. This was expected, as the operating pressure was increased via a larger LP side of the system – combustor boosting.

Case 15 tests the system response and performance to increasing operating pressures via increased compression ratio of the combustor unit instead of its boosting. The results proved this strategy to be inferior compared to the boosting. For details, refer to the Appendix B1. DCEE system at higher pressure (increased CR of the HP side). Case 16 investigated the effects of reintroduced intercooling at the higher pressures, and the results are presented and discussed in the Appendix B2. Reintroduction of the intercooling at higher pressure with a restricted PCP. Again, it is still preferable to avoid intercooling at these pressures. Finally, Appendix B3. DCEE fueled by hydrogen versus diesel, compares the hydrogen combustion to diesel combustion in the DCEE.

8. Summary and conclusions

This computational study investigated a double compression-expansion engine (DCEE) concept fueled by hydrogen (H_2), with a number of potential ways to maximize its efficiency, and the resulting powertrain brake thermal efficiency (BTE) levels. The results were also compared to a diesel version of the same engine. The computations were performed in 1D and 3D using the GT-Power and Converge CFD solvers, respectively. Fig. 12 presents the final predicted efficiencies for all simulated cases sorted in an ascending order of their BTE.

The following conclusions were drawn in this study:

1. A catalytic burner in the exhaust of the combustion cylinder may enable the low-pressure (LP) part of the system to recoup approximately half of the energy lost to incomplete combustion in the combustor unit. In our case, this yielded 1.5 percentage points improvement in the system efficiency.
2. The removal of intercooling after the compressor may improve the system efficiency by 0.3–0.5 percentage points, depending on the pressure levels. This is achieved via a larger LP work.
3. Expander unit insulation may improve the system efficiency by 1.3 percentage points. The compressor insulation is unnecessary as its benefits are marginal.
4. Condensing the water out in the EGR cooler also gives additional 0.8 percentage points increase in the system efficiency when the peak cylinder pressures (PCP) in the combustor are not restricted. The improvements are achieved via improved combustor unit performance (HP side).
5. Raising the HP-to-LP crossover pressure by 25% with no restrictions on the system PCP gave 0.3 percentage points improvement in the system efficiency. This is possible owing to the effective insulation of the expander unit and combustor's exhaust ports. However, this also caused 30 K higher HP tank temperatures, the risks of which should be carefully considered.
6. The system efficiency may be further improved by raising the pressures in the combustion cylinder closer to the base engine's structural limits (300 bar PCP in our case). The system efficiency improvements may reach 1.8 percentage points. The higher pressures should be achieved via a larger LP part of the system, thus effectively further boosting the combustor intake, instead of increasing the compression ratio of the HP side.
7. Higher charge densities at 300 bar PCP significantly slow down the H_2 jet penetration and growth, which in turn cause lower heat release rates and larger incomplete combustion losses with the same injection rate. Thus, the injection rate should be increased with the higher PCPs, ideally via higher injector-cylinder differential pressures (increased from 70 to 100 bar in our case).
8. Wall heat transfer losses increase by up to 30% at the PCP of 300 bar compared to ~ 200 bar, which is mostly due to the overall higher in-cylinder temperatures. Both the compression and expansion strokes make contributions to the larger loss.
9. Due to the intrinsically more difficult mixing with DICI H_2 combustion compared to diesel, the air–fuel equivalence ratio (λ) of 1.2 is too low for H_2 combustion from the system efficiency and HP tank temperature standpoints. Here, the most important factor is the combustion efficiency – minimization of unburned H_2. A λ of about 1.4 seems to offer the optimum tradeoff between the engine load, hence mechanical efficiency, and combustion efficiency, enabling **a BTE of 60.3% at the PCP of 300 bar with CI H_2 combustion**.
10. In general, the most important factors for the system BTE were found to be complete combustion and higher pressures in the combustion cylinder, and engine load.
11. The DCEE system with all the implemented improvements was also tested with diesel fuel. The results showed that the CI H_2 version of the DCEE is likely to achieve in the range of 5–6 percentage points higher brake thermal efficiency compared to the diesel counterpart, which is mostly due to the net molar expansion with H_2 injections at TDC and ~ 50% lower heat transfer losses at these pressures.

CRediT authorship contribution statement

Rafig Babayev: Writing – original draft, Conceptualization, Methodology, Software, Validation, Formal analysis, Investigation, Visualization. **Hong G. Im:** Writing – review & editing, Software, Supervision. **Arne Andersson:** Conceptualization, Supervision, Project administration. **Bengt Johansson:** Writing – review & editing, Conceptualization, Supervision, Project administration, Funding acquisition.

Declaration of Competing Interest

The authors declare that they have no known competing financial interests or personal relationships that could have appeared to influence the work reported in this paper.

Acknowledgments

Babayev R. and Johansson B. would like to thank the Combustion Engine Research Center (CERC) at the Chalmers University of Technology for the financial support. Im H.G. was sponsored by the King Abdullah University of Science and Technology (KAUST). The computations and data handling were enabled by resources provided by the Swedish National Infrastructure for Computing (SNIC) at Chalmers Centre for Computational Science and Engineering (C3SE), partially funded by the Swedish Research Council through grant agreement no. 2018-05973. Additionally, Convergent Science provided CONVERGE licenses and technical support for this work.

Appendix A

(See Tables A1 to A4).

Table A1
Combustion cylinder and injector specifications.

Cylinder bore	131.0 mm
Stroke	158.0 mm
Con. Rod length	267.5 mm
Crank offset	0.0 mm
Compression ratio	11.5: 1
Fuel system	Common-rail direct-injection
Nozzle orifice #	12
Orifice diameter	1 mm
Injector umbrella angle	154°
Pilot injection timing	−10 CA° aTDC
Pilot injection duration	70 μs (0.5 CA° at 1200 RPM)
Pilot injection target fuel mass	1.5 mg
Main injection timing	0 CA° aTDC
Main injection target mass	See Table A. 2
EGR rate	48%
Engine speed	1200 RPM

Table A2
DCEE system geometrical and operational settings for different cases. The arrows illustrate the order of comparison. The parameters that differ significantly between the cases being compared are highlighted in bold.

	Case 1	*Case 2*	*Case 3*	*Case 4*	*Case 5*	*Case 6*	*Case 7*	*Case 8*	*Case 9*	*Case 10*	*Case 11*	*Case 12*	*Case 13*	*Case 14*	*Case 15*	*Case 16*
Compressor bore [mm]	170	170	**163**	170	**162**	170	**152**	170	**149**	170	170	**188**	**192**	**205**	**170**	**194**
Expander bore [mm]	230	230	230	230	230	230	230	230	230	230	230	**260**	260	260	**230**	260
Expander intake event duration [cad]	53	53	53	53	53	53	53	53	**47**	**47**	53	47	47	47	47	47
Compression ratio [-]	11.7	11.7	11.7	11.7	11.7	11.7	11.7	11.7	11.7	11.7	11.7	11.7	11.7	11.7	**15.0**	11.7
Compression HTM [-]	0.6	0.6	0.6	0.6	0.6	0.6	0.6	0.6	0.6	0.6	0.6	0.6	0.6	0.6	0.6	0.6
Expansion HTM [-]	0.4	0.4	0.4	0.4	0.4	0.4	0.4	0.4	0.4	0.4	0.4	**0.39**	**0.35**	0.35	0.35	0.35
Injected fuel mass [mg]	101.1	101.1	**93.5**	101.1	**93.4**	101.1	**93.2**	**113.3**	**88.1**	**113.1**	**101.1**	**137.7**	**131.8**	**100.3**	**103.7**	**134.6**
Injection pressure [bar]	~220	~220	~220	~235	~220	~240	~225	~270	~220	~275	~260	~310	~330	~300	~350	~330
Global λ [-]	1.20	**1.15**	1.15	1.15	1.15	**1.17**	**1.17**	1.17	1.17	1.17	**1.42**	1.17	**1.36**	**2.38**	1.36	1.36

Table A3
Predicted DCEE system parameters for different cases. The arrows illustrate the order of comparison. The parameters that differ significantly between the cases being compared are highlighted in bold.

	Case 1	*Case 2*	*Case 3*	*Case 4*	*Case 5*	*Case 6*	*Case 7*	*Case 8*	*Case 9*	*Case 10*	*Case 11*	*Case 12*	*Case 13*	*Case 14*	*Case 15*	*Case 16*
Combustor inlet T [K]	421.2	421.5	**502.3**	**514.4**	500.6	515.1	**492.9**	**526.3**	493.4	**536.0**	523.2	**559.6**	563.4	**575.0**	**531.3**	**516.9**
Combustor inlet P [bar]	5.49	5.58	**5.85**	**6.43**	5.87	6.54	5.26	6.75	5.24	**7.21**	6.62	**8.57**	**8.82**	**9.54**	**7.00**	**8.47**
Combustion efficiency [%]	97.2	97.2	97.2	97.2	97.2	97.2	97.2	97.2	97.2	97.2	**99.9**	**94.0**	**99.7**	**100.0**	99.7	99.7
Combustor trapped mass [mg]	8415.8	8454.0	**7758.6**	8366.9	7774.2	8502.6	**7344.7**	**8911.9**	**7138.5**	**9174.1**	8897.0	**10810.7**	**11176.7**	**12406.6**	**8996.5**	1149(
Combustor PMP [bar]	148.91	150.97	151.24	**165.42**	151.61	168.40	154.15	**195.58**	152.24	**206.18**	191.07	**228.66**	**235.39**	**256.15**	**257.00**	232.0
Combustor PCP [bar]	200.82	202.89	196.50	**213.96**	196.75	216.54	191.23	**238.63**	**186.23**	**247.44**	**228.40**	**293.68**	295.74	289.75	305.22	295.6
HP tank and Expander inlet T [K]	1023.2	1070.4	**1106.5**	**1115.1**	1108.2	1111.3	**1165.0**	**1188.1**	**1192.2**	**1219.4**	**1110.7**	1227.2	**1150.0**	**955.9**	**1125.8**	**1123.**
HP tank and Expander inlet P [bar]	7.63	**8.18**	**7.57**	8.23	7.74	8.49	**7.34**	**9.11**	**8.74**	**11.47**	**8.66**	**11.03**	**10.74**	**10.00**	**10.56**	10.86
Expander T_{EVO} [K]	627.9	**654.2**	**684.8**	**691.7**	**719.7**	**722.0**	**749.3**	**766.6**	**720.3**	**733.1**	**703.5**	741.1	685.3	550.3	668.3	664.6
Expander P_{EVO} [bar]	1.23	1.28	1.24	1.35	1.30	1.43	1.23	1.53	1.14	1.44	1.39	1.41	1.34	1.19	1.31	1.33

Table A4
Specific NOx emissions estimated from 3D CFD simulations using the extended Zeldovich mechanism.

	Specific NOx emissions [g/kWh]
Case 1 (BTE = 54.1%)	0.1
Case 12 (BTE = 58.7%)	0.7
Case 13 (BTE = 60.3%)	1.9
Case 14 (BTE = 59.4%)	2.0

Appendix B

B1. DCEE system at higher pressure (increased CR of the HP side).

Case 15 vs Case 13.

Alternative way of increasing the peak pressure of the system is via higher compression ratio of the combustion cylinder (HP side), instead of LP side displacement. Fig. A1 (see the Appendix) shows that the system BTE in this scenario is 0.9%-points lower compared to Case 13. The results are very similar to Case 14 in that the NIW is the same as in Case 13, while the BTE is lower due to the larger proportion of fuel energy lost to friction. This is, again, caused by the lower air flow rate through the system at the fixed λ (=1.36), which necessitates lower fueling and engine load.

Another issue with the use of a higher compression ratio piston in the combustion cylinder is the limited space for H_2 jet development. A higher CR would lead to more jet-wall interactions, hence more flame quenching, slower combustion, and larger heat transfer losses. Thus, it is advisable to boost the combustion cylinder via larger LP side displacement for achieving higher operating pressures and BTEs.

B2. Reintroduction of the intercooling at higher pressure with a restricted PCP.

Case 16 vs Case 13.

It was argued previously by Lam et al. [55] that intercooling improves the combustor indicated efficiency. This is because, with the lower intake temperatures the gas density increases, thus raising the λ and allowing for higher fueling. In [33] the benefits of intercooling were shown to be smaller than the losses associated with the lost heat because the intake pressures were allowed to change freely. However, now the PCP, and hence the intake pressure, are limited (PCP_{max} = 300 bar), thus the benefits of intercooling might overweight the drawbacks. This is tested in Case 16, and the results are presented in Fig. A2 (see the Appendix). In this case, the combustor unit intake temperature is limited at 250 °C instead of the previously attained 300 °C with Case 13.

The results show that, even though the gross indicated efficiency of the HP side increased as expected in Case 16 with intercooling, the LP work reduced significantly due to heat rejected by the CAC. The proportion of friction losses reduced marginally owing to the higher engine load; however, the negative effects override the positive, leading to 0.3%-points lower system BTE compared to Case 13. This shows that it is still preferable from the efficiency standpoint to avoid intercooling in the DCEE even when the PCP is limited at 300 bar.

B3. DCEE fueled by hydrogen versus diesel.

In this section, the hydrogen combustion Case 13 with the best system efficiency of 60.3% is compared to equivalent diesel version. The PCP is maintained at around 300 bar. Two diesel cases are considered, the first one with the same HTMs and combustion efficiency as in the hydrogen Case 13, and the second one with these parameters adjusted. The adjusted values for the HTMs are taken from [33], and they are close to unity in the expansion stroke. The adjusted combustion efficiency is assumed to equal 99.9%, in accordance with the previously reported values for diesel.

The first diesel case with fixed HTMs and combustion efficiency is used to analyze the effects of the changed fuel only, while the second diesel case is used for more realistic system efficiency estimations. Fig. B1 suggests that using liquid diesel fuel instead of gaseous hydrogen in itself leads to 1.5%-point reduction in the system BTE. This demonstrates the benefit of having to inject a large mole number of the low-density hydrogen at TDC, which leads to a net molar expansion. The amount of work generated by these additional moles was estimated in [23] to be in the range of 2–4% of the injected fuel chemical energy. Injecting diesel also adds more moles but the number is 30 times smaller than with H_2 [23], giving no appreciable difference. However, diesel combustion has a molar expansion ratio of 1.056 [56], which also provides molar expansion work, but its contribution is estimated to be half of that from the H_2 injections at TDC [23]. Considering the proportion of the brake system work generated in the combustor unit, the 1.5%-points higher efficiency with hydrogen seems to agree well with the previous conclusions on the mole number effects. Another contributing factor, albeit a smaller one, is the heat of vaporization of the liquid diesel fuel, which is estimated to be in the range of 0.7% of the injected fuel energy. The loss of heat in the cylinder due to vaporization is avoided with the gaseous H_2 fuel, thus giving additional contribution to the improved efficiency, even though some of it is lost to the heating of the H_2 gas by the hotter in-cylinder air.

The second diesel case with more realistic HTMs and combustion efficiency is estimated to yield 5.8%-points lower system BTE compared to the H_2 case. Apart from the molar and fuel vaporization/heating effects, the difference is largely due to the heat transfer losses in the combustion cylinder with diesel, which are in the range of 14.7% of the total fuel energy versus 7.5% with H_2. This also demonstrates the importance of the combustion system optimization path that was developed specifically for DICI H_2 engines in Babayev et al. [24] for achieving a BTE close to or above 60%. These levels of wall heat transfer are not realizable with conventional diesel combustion as that would require drastically lowering the injection pressures, which would lead to slower burning, hence lower efficiency, and unacceptable soot emissions. Furthermore, a maximum BTE of 55% was reported in [33] with the diesel combustion, which suggests that the diesel version of the DCEE does not respond equally favorably to the system improvements recommended in this work for the H_2 combustion.

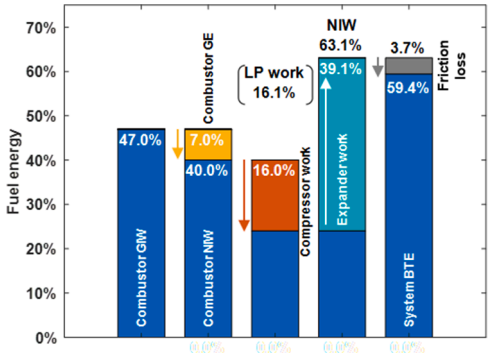

Fig. A1. Different components of the DCEE system energy flow at a PCP of 300 bar achieved via increased CR of the combustor unit (Case 15).

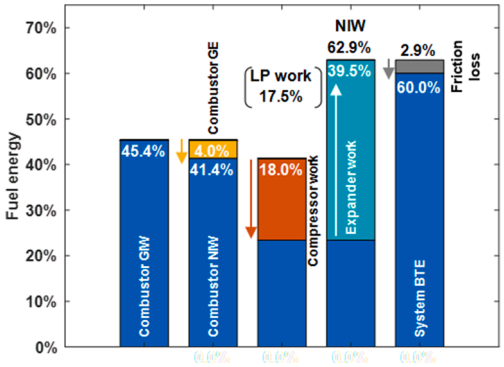

Fig. A2. Different components of the DCEE system energy flow with reintroduced intercooling at a PCP of 300 bar (Case 16).

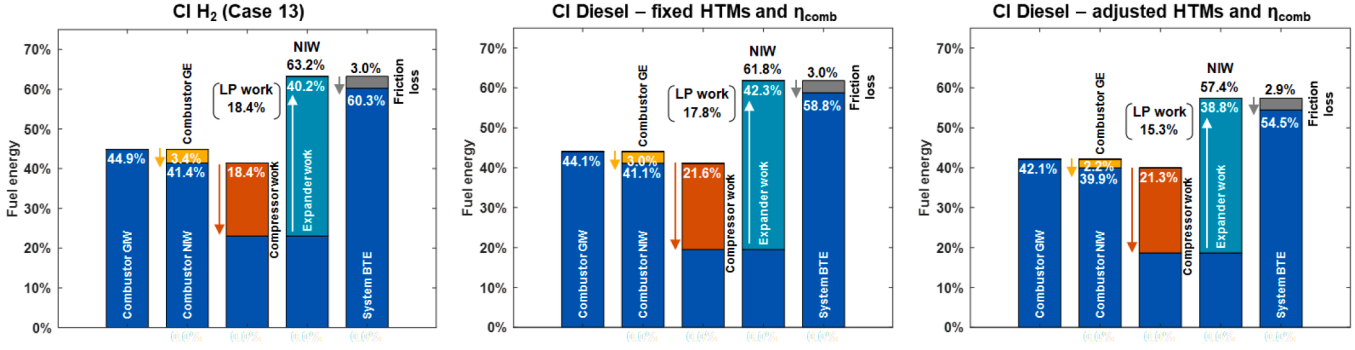

Fig. B1. Different components of the DCEE system energy flow at a PCP of 300 bar with diesel versus hydrogen as fuel.

Appendix C

(See Fig. C1).

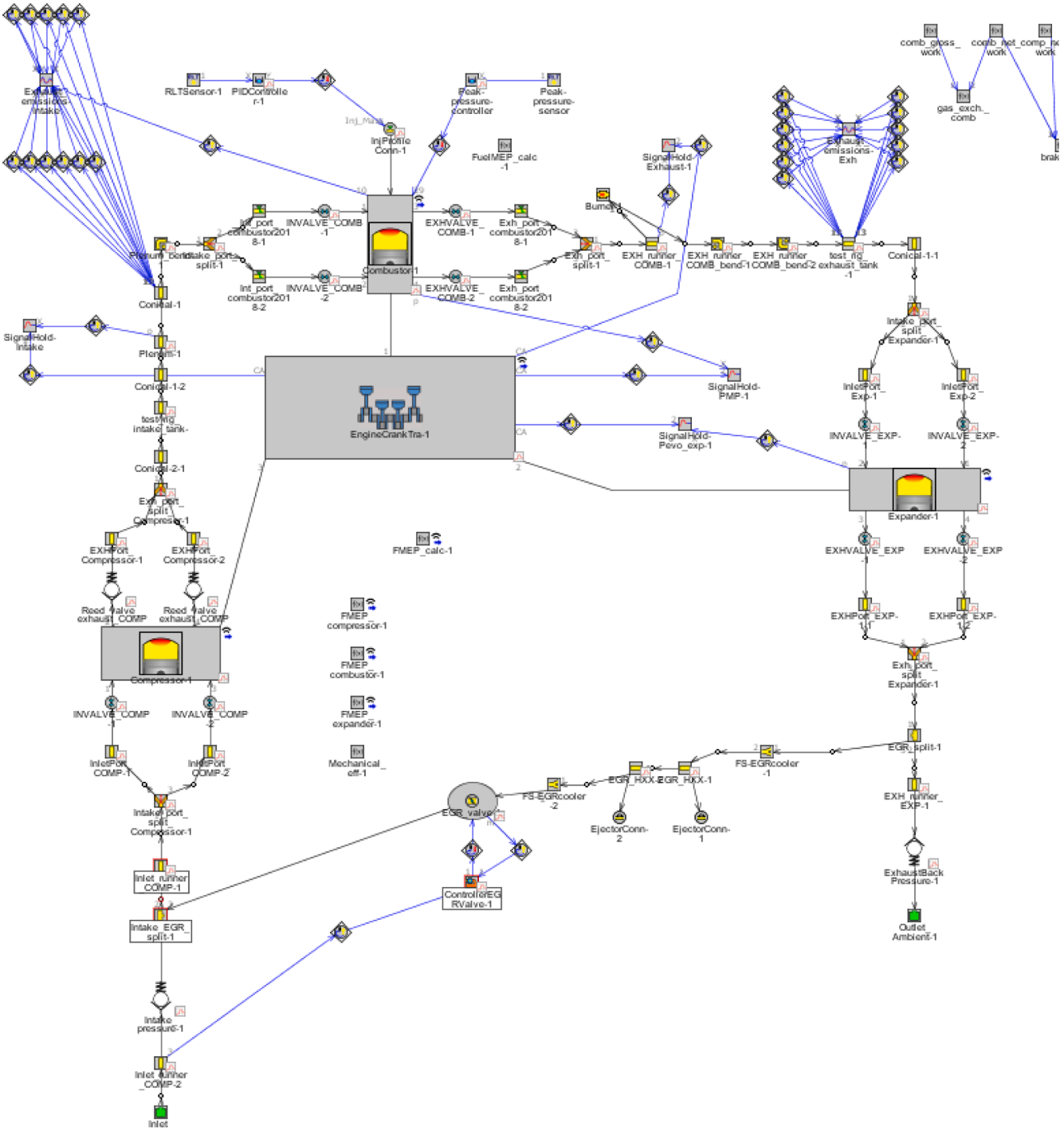

Fig. C1. The 1D model layout in the GT-Power software GUI.

References

[1] Council H. Hydrogen Insights–A perspective on hydrogen investment, market development and cost competitiveness 2021.
[2] Kurtz JM, Sprik S, Saur G, Onorato S. Fuel cell electric vehicle durability and fuel cell performance. National Renewable Energy Lab.(NREL), Golden, CO (United States); 2019.
[3] Göhring E, von Glasner E-C, Povel R. Engine braking systems and retarders-an overview from an european standpoint. SAE Technical Paper 1992. https://doi.org/10.4271/922451.
[4] Thompson ST, James BD, Huya-Kouadio JM, Houchins C, DeSantis DA, Ahluwalia R, et al. Direct hydrogen fuel cell electric vehicle cost analysis: System and high-volume manufacturing description, validation, and outlook. J Power Sources 2018;399:304–13.
[5] Cox B, Bauer C, Mendoza Beltran A, van Vuuren DP, Mutel CL. Life cycle environmental and cost comparison of current and future passenger cars under different energy scenarios. Appl Energy 2020;269:115021.
[6] Das L. Hydrogen engines: a view of the past and a look into the future. Int J Hydrogen Energy 1990;15(6):425–43.
[7] Verhelst S, Wallner T. Hydrogen-fueled internal combustion engines. Prog Energy Combust Sci 2009;35(6):490–527.
[8] Verhelst S. Recent progress in the use of hydrogen as a fuel for internal combustion engines. Int J Hydrogen Energy 2014;39(2):1071–85.
[9] White C, Steeper R, Lutz A. The hydrogen-fueled internal combustion engine: a technical review. Int J Hydrogen Energy 2006;31(10):1292–305.
[10] Berckmüller M, Rottengruber H, Eder A, Brehm N, Elsässer G, Müller-Alander G, et al. Potentials of a charged SI-hydrogen engine. SAE Technical Paper 2003. https://doi.org/10.4271/2003-01-3210.
[11] Кавтарадзе РЗ, Сун Б, Голосов АС, Чэн Ж, ЧЖан Ц, Чилашвили ГВ. Эффективные показатели водородного двигателя с Модифицированной системой топливоподачи при работе на обеднённой смеси. Труды НАМИ 2021:58–66.
[12] Байган С, Голосов АС, ЖунЖун Ч. Кавтарадзе Реваз Зурабович, д-р техн. наук, профессор1 n.d.
[13] Millo F, Rolando PA, Accurso F, Gullino F, Roggio S, Pesce F, et al. Synergetic application of 0/1/3D-CFD approaches for hydrogen-fuelled spark ignition engine simulation. SAE Int J Engines 2022.
[14] Yip HL, Srna A, Yuen ACY, Kook S, Taylor RA, Yeoh GH, et al. A review of hydrogen direct injection for internal combustion engines: towards carbon-free combustion. Appl Sci 2019;9(22):4842.
[15] Li H, Karim GA. Knock in spark ignition hydrogen engines. Int J Hydrogen Energy 2004;29:859–65.
[16] Mohammadi A, Shioji M, Nakai Y, Ishikura W, Tabo E. Performance and combustion characteristics of a direct injection SI hydrogen engine. Int J Hydrogen Energy 2007;32(2):296–304.
[17] Yu X, Guo Z, He L, Dong W, Sun P, Du Y, et al. Experimental study on lean-burn characteristics of an SI engine with hydrogen/gasoline combined injection and EGR. Int J Hydrogen Energy 2019;44(26):13988–98.
[18] Seboldt D, Mansbart M, Grabner P, Eichlseder H. Hydrogen engines for future passenger cars and light commercial vehicles. MTZ Worldw 2021;82(2):42–7.
[19] Pauer T, Weller H, Schünemann E, Eichlseder H, Grabner P, Schaffer KM. H2 ICE für zukünftige PKWs und leichte Nutzfahrzeuge. Wiener Mot.: VDI Verlag GmbH; 2020. p. 246–63.
[20] Zabetakis MG. Flammability characteristics of combustible gases and vapors. Bureau of Mines Washington DC; 1965.
[21] Law CK. Combustion physics. Cambridge university press; 2010.
[22] Babayev R, Andersson A, Dalmau AS, Im HG, Johansson B. Computational characterization of hydrogen direct injection and nonpremixed combustion in a compression-ignition engine. Int J Hydrogen Energy 2021;46(35):18678–96.
[23] Babayev R, Andersson A, Serra Dalmau A, Im HG, Johansson B. Computational comparison of the conventional diesel and hydrogen direct-injection compression-ignition combustion engines. Fuel 2022;307:121909.
[24] Babayev R, Andersson A, Serra Dalmau A, Im HG, Johansson B. Computational optimization of a hydrogen direct-injection compression-ignition engine for jet mixing dominated nonpremixed combustion. Int J Engine Res 2022;23(5):754–68.
[25] Ikegami M, Miwa K, Shioji M. A study of hydrogen fuelled compression ignition engines. Int J Hydrogen Energy 1982;7(4):341–53.
[26] Eichlseder H, Spuller C, Heindl R, Gerbig F, Heller K. Konzepte für die dieselähnliche Wasserstoffverbrennung. MTZ-Motortechnische Zeitschrift 2010;71(1):60–6.
[27] Naber JD, Siebers DL. Hydrogen combustion under diesel engine conditions. Int J Hydrogen Energy 1998;23:363–71.
[28] Rottengruber H. Investigation of a direct injection hydrogen diesel-engine. Hydrog Energy Prog XII 1998;2:1515.
[29] Koch DT, Sousa A, Bertram D. H2-engine operation with EGR achieving high power and high efficiency emission-free combustion. SAE Technical Paper 2019. https://doi.org/10.4271/2019-01-2178.
[30] Kavtaradze R, Natriashvili T, Gladyshev S. Hydrogen-Diesel engine: problems and prospects of improving the working process. SAE Technical Paper 2019. https://doi.org/10.4271/2019-01-0541.
[31] Natriashvili T, Kavtaradze R, Glonti M. Improvement of ecological characteristics of the hydrogen diesel engine. IOP Conf Ser: Mater Sci Eng 2018;315:012018.
[32] Heindl R, Eichlseder H, Spuller C, Gerbig F, Heller K. New and Innovative Combustion Systems for the H_2–ICE: Compression Ignition and Combined Processes. SAE Int J Engines 2009;2:1231–50.
[33] Babayev R, Andersson A, Dalmau AS, Im HG, Johansson B. Double compression-expansion engine (DCEE) fueled with hydrogen: preliminary computational assessment. Transp Eng 2022;8:100103.
[34] Lam N, Tuner M, Tunestal P, Andersson A, Lundgren S, Johansson B. Double compression expansion engine concepts: a path to high efficiency. SAE Int J Engines 2015;8(4):1562–78.
[35] Lam N, Andersson A, Tunestal P. Double compression expansion engine concepts: efficiency analysis over a load range. SAE Technical Paper 2018. https://doi.org/10.4271/2018-01-0886.
[36] Lam N, Tunestal P, Andersson A. Simulation of system brake efficiency in a double compression-expansion engine-concept (DCEE) based on experimental combustion data. SAE Technical Paper 2019. https://doi.org/10.4271/2019-01-0073.
[37] Shankar VSB, Johansson B, Andersson A. Double compression expansion engine: a parametric study on a high-efficiency engine concept. SAE Technical Paper 2018. https://doi.org/10.4271/2018-01-0890.
[38] Shankar VSB, Lam N, Andersson A, Johansson B. Optimum heat release rates for a double compression expansion (DCEE) engine. SAE Technical Paper 2017. https://doi.org/10.4271/2017-01-0636.
[39] Lou ZD, Deng Q, Wen S, Zhang Y, Yu M, Sun M, et al. Progress in camless variable valve actuation with two-spring pendulum and electrohydraulic latching. SAE Int J Engines 2013;6(1):319–26.
[40] Zwinkels MFM, Järås SG, Menon PG, Griffin TA. Catalytic materials for high-temperature combustion. Catal Rev Eng 1993;35(3):319–58.
[41] https://www.gtisoft.com/gt-suite-applications/propulsion-systems/gt-power-engine-simulation-software/ n.d.
[42] Colburn AP. A method of correlating forced convection heat transfer data and a comparison with fluid friction. Trans Am Inst Chem Engrs 1993;29:174–210.
[43] Morel T, Keribar R. A model for predicting spatially and time resolved convective heat transfer in bowl-in-piston combustion chambers. SAE Trans 1985:77–93.
[44] Woschni G. A universally applicable equation for the instantaneous heat transfer coefficient in the internal combustion engine. SAE Technical paper 1967. https://doi.org/10.4271/670931.
[45] Megel M, Westmoreland B, Jones G, Phillips F, Eberle D, Tussing M, et al. Development of a structurally optimized heavy duty diesel cylinder head design capable of 250 bar peak cylinder pressure operation. SAE Int J Engines 2011;4(3):2736–55.
[46] Crabb D, Fleiss M, Larsson J-E, Somhorst J. New modular engine platform from Volvo. MTZ Worldw 2013;74(9):4–11.
[47] Metzner FT, Becker N, Demmelbauer-Ebner W, Müller R, Bach MW. Der neue 6-l-W12-Motor im Audi A8. MTZ-Motortechnische Zeitschrift 2004;65(4):254–66.
[48] [48] Noble A, Such C. Ways to reduce CO2 emissions from on-highway, heavy duty diesel engines. Transp. Res. Arena 5th Conf. Transp. Solut. from Res. to DeploymentEuropean Comm. Eur. Dir. Roads Eur. Road Transp. Res. Advis. Counc. WATERBORNE^{TP}European Rail Res., 2014.
[49] Knauder C, Allmaier H, Sander DE, Sams T. Investigations of the friction losses of different engine concepts. part 1: a combined approach for applying subassembly-resolved friction loss analysis on a modern passenger-car diesel engine. Lubricants 2019;7:39.
[50] Senecal PK, Pomraning E, Richards KJ, Briggs TE, Choi CY, McDavid RM, et al. Multi-dimensional modeling of direct-injection diesel spray liquid length and flame lift-off length using CFD and parallel detailed chemistry. SAE Trans 2003:1331–51.
[51] Richards KJ, Senecal PK, Pomraning E. CONVERGE 3.0. Converg Sci Madison, WI 2000.
[52] McTaggart-Cowan G, Mann K, Huang J, Singh A, Patychuk B, Zheng ZX, et al. Direct injection of natural gas at up to 600 bar in a pilot-ignited heavy-duty engine. SAE Int J Engines 2015;8(3):981–96.
[53] Burke MP, Chaos M, Ju Y, Dryer FL, Klippenstein SJ. Comprehensive H_2/O_2 kinetic model for high-pressure combustion. Int J Chem Kinet 2012;44(7):444–74.
[54] Knop V, Benkenida A, Jay S, Colin O. Modelling of combustion and nitrogen oxide formation in hydrogen-fuelled internal combustion engines within a 3D CFD code. Int J Hydrogen Energy 2008;33(19):5083–97.
[55] Lam N, Tunestal P, Andersson A. Analyzing factors affecting gross indicated efficiency when inlet temperature is changed. SAE Technical Paper 2018. https://doi.org/10.4271/2018-01-1780.
[56] Nguyen D-K, Szybist J, Sileghem L, Verhelst S. Effects of molar expansion ratio of fuels on engine efficiency. Fuel 2020;263:116743. https://doi.org/10.1016/j.fuel.2019.116743.